Acoustic feedbacks of loudspeaker-room-microphone environments with directivity

Diploma Thesis

by

Nadine Kroher

Supervisor: Dr. Franz Zotter

Assessor: O.Univ.Prof. Mag.art DI Dr.techn. Robert Höldrich

Graz, May 2011

Institute of Electronic Music and Acoustics

University of Music and Performing Arts, Graz – Austria

DECLARATION

Pledge of Integrity

I hereby certify that the work presented in this thesis is my own, that all work performed by others is appropriately declared and cited, and that no sources other that those listed were used.

Eidesstattliche Erklärung

Ich versichere ehrenwörtlich, dass ich diese Arbeit selbständig verfasst habe, dass sämtliche Arbeiten von anderen entsprechend gekennzeichnet und mit Quellenangaben versehen sind und dass ich keine anderen als die angegebenen Quellen verwendet habe.

Place: _____

Date: _____

Signature: _____

ABSTRACT

Everybody is familiar with the unwanted howling sound of acoustic feedbacks in public adress systems or at live-concerts. Especially in monitoring situations, where a large amount of the radiated sound is fed back into the microphone, howling, also known as the *Larsen* effect, occurs quite often. Ironically, this unwanted sound has been used in many movie soundtracks to express the presence of a sound reinforcement system. Literature on acoustic feedback has focused on diffuse sound fields, phase and amplitude conditions under which feedbacks occur. Directivity was usually only taken into account statistically, considering the directivity index.

The aim of this thesis is to develop a feedback simulation which includes measured complex directivity patterns of both the loudspeaker and the microphone. Therefore a simple acoustic mirror source room model is used to simulate the direct sound path as well as the wall reflections including the directivity in magnitude and phase. Hereby, the impact of several factors can be investigated: Orientation and location of source and microphone, the directivity factor and room and absorption parameters.

The simulation results are evaluated for several situations regarding their plausibility and the usability for feedback estimation in different applications. Finally, to investigate the general behavior of feedback-prone systems and to find adequate simulation methods, the influence of several parameters of the simulation shall be isolated or simplified: For instance, the impact of phase data in the directivity patterns and the influence of the reflected sound in comparison to the direct path.

KURZFASSUNG

Es ist allgemein bekannt, dass akustische Rückkopplungen in Beschallungsanlagen oder bei Live-Konzerten unerwünschte Pfeiftöne verursachen. Besonders in Monitor-Situationen gelangt ein großer Teil des abgestrahlten Schalls zurück ins Mikrofon, wodurch das störende, auch als *Larsen*-Effekt bezeichnete, Geräusch hörbar wird. Paradoxerweise wird genau dieser Effekt sehr häufig im Filmton verwendet, um das Vorhandensein einer Beschallungsanlage zu suggerieren. In der vorhandenen Literatur wurden bereits die Gegebenheiten bzgl. Diffusschallfeld, Phase und Amplitude erforscht, unter welchen akustische Rückkopplungen bevorzugt auftreten. Die Richtwirkung wurde allerdings weitestgehend nur durch den Richtungsindex, also rein statistisch, berücksichtigt.

Ziel dieser Arbeit ist die Entwicklung einer Simulation der Rückkopplungsneigung, welche auch die gemessenen Richtcharakteristiken von Lautsprecher und Mikrofon berücksichtigt. Hierzu wird ein Spiegelquellen-Modell eines einfachen Raumes verwendet, um den direkten Schallweg, sowie die Reflexionen in Betrag und Phase zu simulieren. Somit kann der Einfluss einzelner Faktoren untersucht werden, z.B. Platzierung und Ausrichtung von Mikrofon und Lautsprecher, verwendete Richtcharakteristiken, sowie der Einfluss von Raum- und Absorptionsparametern.

Die Simulationsergebnisse für diverse Szenarien werden auf ihre Plausibilität und Verwendbarkeit für unterschiedliche Anwendungen hin untersucht. Abschließend werden einzelne Simulationsparameter abgetrennt oder vereinfacht, um allgemeine Aussagen über die Rückkopplungsneigung zu erlangen und geeignete Simulationsmethoden zu finden. Hierzu zählt beispielsweise die Bedeutung der Phaseninformation in den Richtcharakteristiken oder der Einfluss des reflektierten Schalls im Vergleich zum Direktschall.

AKNOWLEDGEMENTS

My sincere thanks go to my supervisor Franz Zotter for his dedication and for keeping me motivated with his sense of humor and his easy-going way of dealing with abstract scientific issues.

I thank my fellow students Clara and Jamilla for the commonly occurring and diverting conversations on social science over a glass of wine or two.

I thank my friend Claudia for „climbing Machu Picchu“ to share her entertaining NY-style worldview with me.

I thank my roommates Peter, Djamil, Meret and Viktor for sharing this tremendous time in our bohemian shack.

I thank Karin, Jürgen and Lars for being like a family to me.

Dedicated to Cyril. Thank your for your love and care and for preparing great coffee.

„Don´t worry! Where would rock ´n´ roll be without feedback“

– David Gilmour after the recording engineer cuts the playback because of feedback problems

CONTENTS

Chapter 1

INTRODUCTION

The occurrence of unwanted howling effects due to acoustic coupling is in most cases the limiting factor for the employable gain in sound reinforcement systems. A common method of increasing the maximum gain before instability is to manually equalize the overall transfer function of the system. Various automatic methods, as phase- or frequency modulation, howling detection, automatic gain reduction, spatial filtering and room modeling methods have been outlined in [WM09]. While recent investigation focuses more on the automatic detection and suppression of acoustic feedbacks, the investigation of the behavior of feedback-prone systems was carried out in the 1960s and 70s. [BB66] examined the behavior of the system response itself, while [Kle73] and [Sch71] investigated the influence of the components of the sound reinforcement system on the behavior of the overall system. One of the first modern simulation concepts using mirror sources and directivity patterns was carried out by [TR09].

The aim of this thesis is to investigate the behavior of feedback prone systems with up-to-date methods by simulating a loudspeaker-room-microphone model. For this purpose, an accurate directivity pattern of both, microphone and loudspeaker, is interpolated using circular harmonic basis functions. Furthermore, early reflections are taken into consideration by applying a simple mirror source model, including the absorption coefficients of wall surfaces. This way, the overall transfer function of the system can be obtained and the maximum gain before instability can be estimated for different scenarios. This method also provides information about the frequency at which feedback occurs and the impact of the different propagation paths on the overall frequency response.

Preview of this thesis

Chapter 2 reviews the theory on acoustic feedbacks and gives detailed information on the particular components of the simulation: The interpolation of the measured directivity pattern, the implementation of the image source method, the time delay and amplitude attenuation between sources and microphone, wall reflection and the calculation and analysis of the loop transfer function.

Chapter 3 shows the simulation results of different scenarios and under the absence or modification of various simulation components. Hence general conclusions about the behavior of the overall and the loop transfer function are drawn.

Chapter 4 provides a short summary of the achievements of this work and deals with the perspectives given by this method as well as its limitations. Furthermore, suggestions for future work on this topic are proposed.

Chapter 2

THEORY ON ACOUSTIC FEEDBACK NETWORKS AND SIMULATION COMPONENTS

2.1. Incurrence of Acoustic Feedbacks

In every sound reinforcement system, where the loudspeaker and the microphone are placed in the same acoustic environment, a certain amount of the signal radiated by the loudspeaker is fed back into the microphone. In [Fig.2.1] a simple loudspeaker-room-microphone model is shown, where s(t) represents the input sound signal, e.g, a person speaking in front of the microphone, w(t) the sound captured by the microphone and r(t) the sound radiated by the speaker. The amplification of the input signal is modeled as a broadband gain factor g and the loop gain as a frequency-dependent transfer function L(ω).

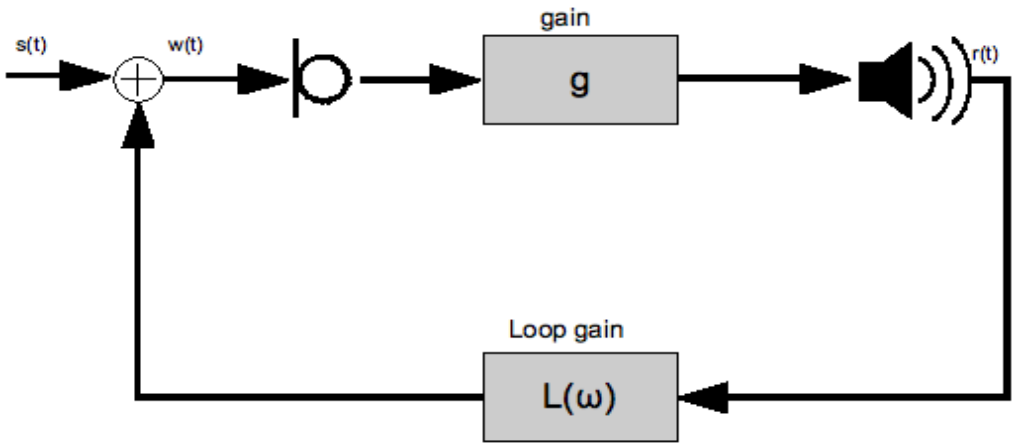

Fig. 2.1: Simplified speaker-room-microphone model

The signal captured by the microphone, w(t), can be calculated as

(2.1) $$r = w \cdot g = (s + L \cdot r) \cdot g = s \cdot g + L \cdot r \cdot g \quad ,$$

which leads to the overall transfer function:

(2.2) $$H = \frac{r}{s} = \frac{g}{(1 - L \cdot g)} \quad .$$

If the described System becomes unstable, howling, also known as the *Larsen* effect, occurs. According to the *Nyquist stability criterion* [Nyq32], a System H becomes unstable, when two conditions are fulfilled concurrently at at least one frequency:

The product of the gain and the magnitude of the loop transfer function is greater or equal 1

(2.3) $$|(L \cdot g)| \geq 1 \quad ,$$

and the phase at this frequency is an integer of 2π

(2.4) $$\sphericalangle(L) = n \cdot 2 \cdot \pi \quad for \quad n = 1,2,3,4,... \quad .$$

2.2. Maximum stable gain

As described in eq. (2.3.), the applicable gain before the system becomes unstable is limited by the magnitude of the peak of the loop transfer function L, at which the phase is a multiple of 2π. Since the phase usually changes rapidly over the frequency, the peak of the magnitude is a good indicator for the applicable gain before instability, as also experimentally observed in [BB66]: Even if the phase condition is not fulfilled at the frequency of the peak, it will be at a close frequency, which is still in the slope of the peak and the error due to the omission of the phase criterion is in many cases fairly small.

For a loudspeaker and a microphone in an anechoic chamber, arranged with the main axises to each other, the phase at the microphone is related to the distance d between

them as follows:

$$\varphi = 2 \cdot \pi \cdot f \cdot \Delta t = \frac{2 \cdot \pi \cdot f \cdot d}{c} \quad , \tag{2.5}$$

where c represents the speed of sound.

Accordingly, the distance, at which a phase change of 2π takes place within a frequency range of 100 Hz, can be calculated:

$$\varphi 2 - \varphi 1 = 2 \cdot \pi = \frac{(f2 - f1) \cdot 2 \cdot \pi \cdot d}{c} \quad , \tag{2.6}$$

$$d = \frac{c}{\Delta f} = \frac{343\,(m/s)}{100\,Hz} = 3{,}43\,m \quad . \tag{2.7}$$

Of course, under the presence of reflections, the behavior of the phase becomes more complex. Besides, also the microphone and the loudspeaker have a non-zero phase response. This issue will be further discussed in *Chapter 3* and it will be demonstrated that in many cases the magnitude condition provides a good estimation of the maximum stable gain and the frequency range at which feedback occurs, when the linear open loop response is known. If the exact frequency is of interest, the phase criterion has to be taken into consideration.

The *maximum stable gain* (MSG) is a measure for the system and is defined for a broadband gain factor as:

$$MSG = -20 \cdot \log(max|L|) \quad . \tag{2.8}$$

The paper [WM09] suggests for practical applications a headroom of 2 to 3 dB to avoid audible artifacts. This could also be verified in an acoustic feedback simulation in P*ure Data* (*Chapter 2.11*). When increasing the gain towards the before determined maximum stable gain, annoying artifacts can be heard. Gain factors above the MSG produce the audible *Larsen* effect, the howling known from public adress systems.

Continuous-time systems

The stability of continuous-time systems can be analyzed in the s-domain: A system is stable, if all poles are located within the left half-plane. For example, let L(s) be the loop transfer function with the pole at -p:

(2.9) $$L(s)=\frac{1}{s+p} \quad .$$

Placing the loop transfer function within the feedback network with the gain g, the resulting overall transfer function H(s) can be calculated:

(2.10) $$H(s)=\frac{g}{1-g\cdot L(s)}=\frac{g\cdot(s+p)}{s+(p-g)} \quad .$$

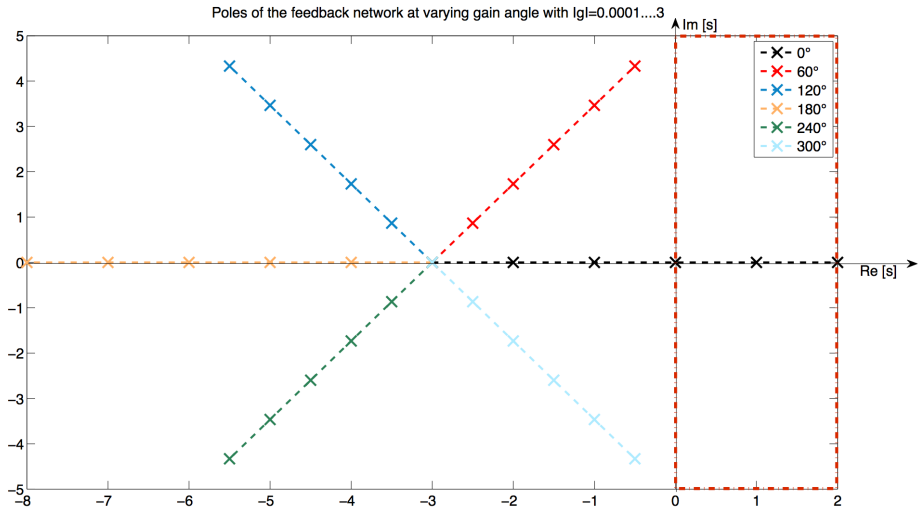

Fig.2.2: poles of the overall transfer function for different komplex gain values

The pole of the overall transfer function is now located at -(p-g). [Fig. 2.2] shows the pole-zero plot for a lowpass filter with one pole at p=-3 placed in a feedback network. If a scalar gain is increased above the feedback limit, the pole is moved to the right half-plane and the system becomes unstable. When a complex gain with a non-zero phase is increased, the system reamins stable also for absolute values above the feedback limit. For a phase between -90° and 90°, instability occurs at higher gain values.

Discrete-time systems

For discrete-time systems, the location of the poles in the z-domain, gives information about stability. A discrete-time system is stable, if its poles are located within the unit circle. For example, a digital lowpass-filter with the transfer function L(z) has one pole at z=0.9:

(2.11) $$L_{lowpass}(z) = \frac{1}{1 - 0.9 \cdot z^{-1}} \quad .$$

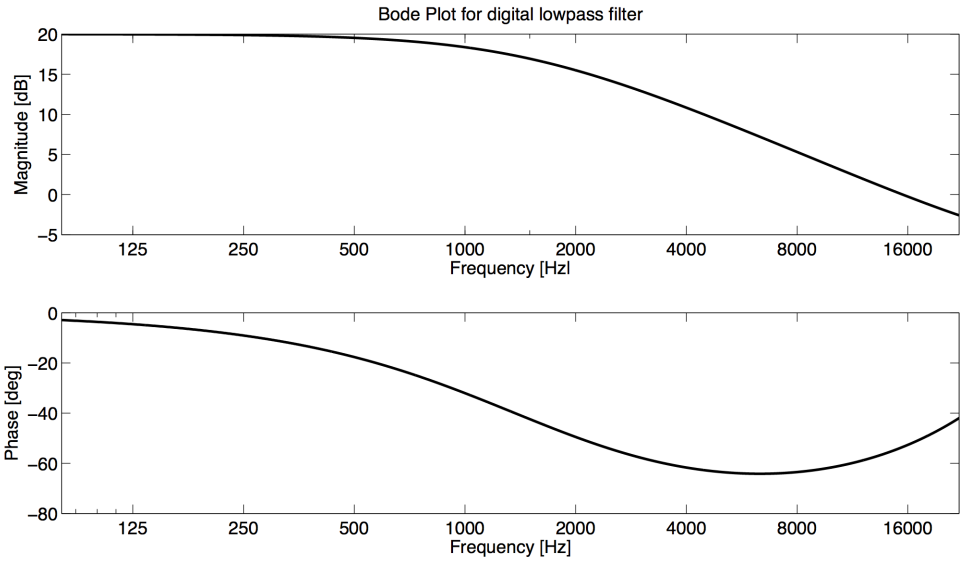

Fig. 2.3: Bode plot of the lowpass filter

[Fig. 2.3] shows the bode plot of the filer. Let us asume, that the filter is placed as a loop transfer function in a feedback network as described in [Fig. 2.1]. Resulting from the magnitude of 20dB and the zero-phase for low frequencies, the feedback limit for a scalar gain in the feedback network is g=0.1:

(2.12) $$MSG_{dB} = -20 * log10\left[max\left|\left(L_{cheb}(f)\right)\right|\right] = -20\text{dB} \quad ,$$

(2.13) $$MSG = 10^{\left(\frac{MSG_{dB}}{20}\right)} = 0.1 \quad .$$

[Fig. 2.4] shows the pole-zero-map of the overall system. Discrete-time systems are

stable, when all poles are located within the unit circle. When a scalar gain is increased below the feedback limit, the pole is being relocated. For a scalar gain of g=0.1, the pole is moved slightly outside the unit circle and the system becomes unstable. When a complex gain with a phase other than 0° is used, the system becomes unstable for higher gain values than the MSG.

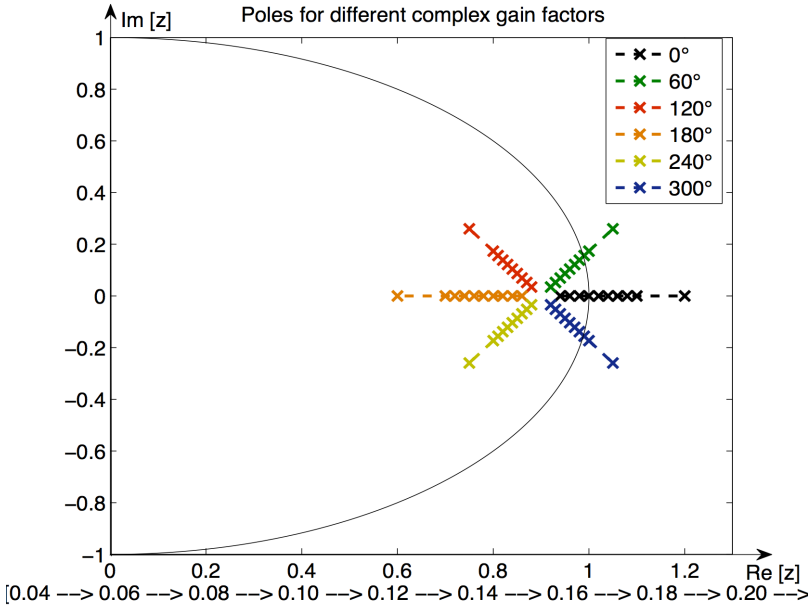

(a) complex gain factors

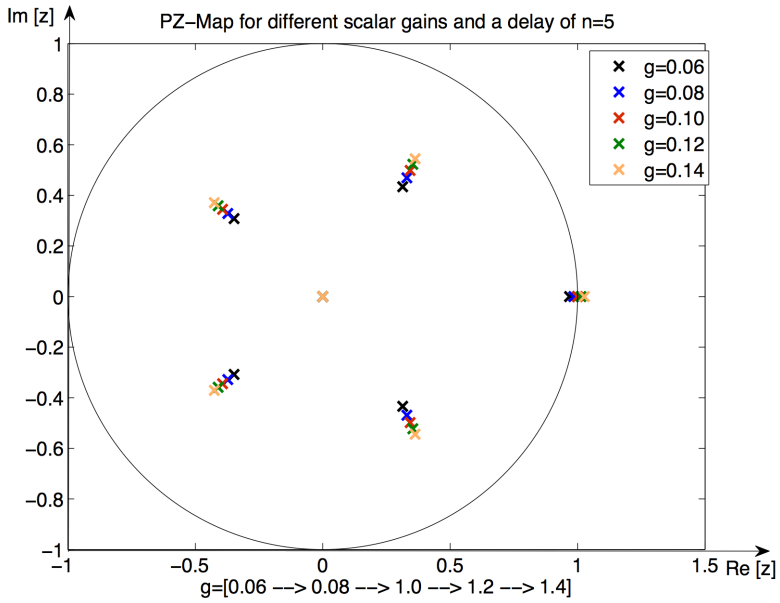

(b) scalar gain factors for N=5

Fig. 2.4: P/Z plot of the filter within the feedback

The feedback path of a discrete-time system always has to be delayed by at least one sample. If the delay N is increased, also the number of poles N+1 increases, as shown in [Fig. 2.4 (b)].

To analyse stability in the z-domain, the transfer function has to be decomposed into linear factors in order to determine poles an zeros. While this procedure is quite simple for transfer functions with few coefficients as in the example above, it turned out to be numerically too complex to perform this action for the room simulation, where the overall impulse response has a length of more than 22,000 points. Even for 100 coefficient, the task is already very time-consuming.

Fourier transform and causality

Another option to investigate stability of a feedback network, is to take a closer look at the inverse Fourier transform of the overall transfer function H(f). As mentioned before, if a system is causal and stable, its poles are within the unit circle. Non-causal, stable systems on the other hand have their poles outside the unit circle. Since stability is a requirement for the Fourier transform, the inverse Fourier transform of an unstable system will result in a non-causal impulse response, i.e. the impulse response will show components at n<0 which increase towards zero.

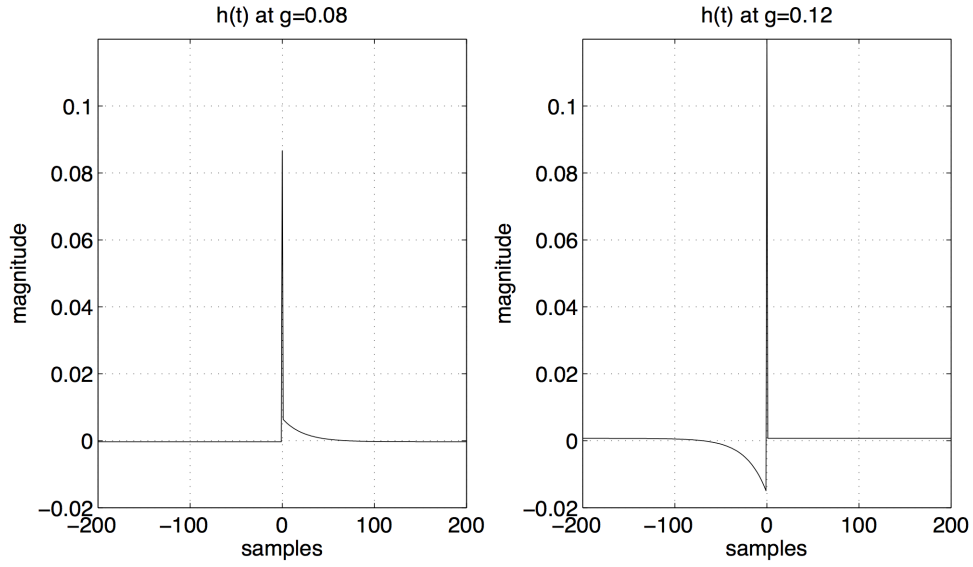

Fig. 2.5: inverse fourier transform of H(f) with MSG=0.1; (a) g=0.08; (b) g=0.12

Investigating the stability with this method has shown similar results as the calculated stability with the *Nyquist* magnitude criterion. [Fig. 2.5] shows the impulse response h(t) of a system with a calculated MSG of g=0.1. When applying a gain of g=0.08, the impulse response does not show any non-causal components. Increasing the gain to g=0.12, strong components for n<0 can be observed.

2.3. Measurement of the complex angle-dependent impulse responses

For the simulation, an existing set of measurement data of the angle-dependent, complex impulse responses of four dynamic super-cardioid microphones was used: An *AKG P5*, an *AKG D7*, a Neumann *KMS105* and a Shure *KSM 9*. In addition, measurements of a dynamic cardioid (*Shure SM58*), a condenser cardioid (*AKG C480B*) and a directive shotgun microphone (*AKG CK98* with *SE300B* power supply) were realized. These measurements were carried out at the IEM multi-channel measurement station, placing the microphone on a rotary plate and recording the test signal played by a fixed speaker.

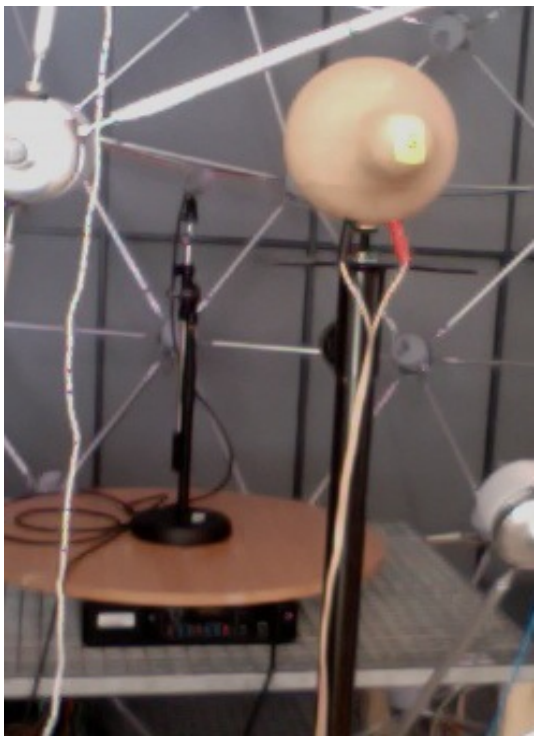

Fig. 2.6.: Setup for microphone impulse response measurement

Exponential sweep measurement

Because of its high robustness to distortions and background noise, an exponential sweep measurement, as described in [Far08], was used. The instantaneous frequency Ω[n] of the sweep signal x[n] of the duration N with the start- and stop-frequencies ω_0 and ω_1 is given by:

$$\Omega[n] = \omega_0 \cdot \left(\frac{\omega_0}{\omega_1} \right)^{\left(\frac{n}{N-1}\right)} \quad , \tag{2.14}$$

and the sweep x[n] by:

$$x[n] = \sin(\phi[n]) \quad , \tag{2.15}$$

with

$$\Phi[n] = \sum_{n=0}^{N} \Omega[n] \quad . \tag{2.16}$$

From the recorded impulse responses y[n], the microphone impulse responses can be obtained by filtering with the inverse frequency response of the test signal x[n]:

$$m[\varphi_i, n] = F^{-1}\left(\frac{F(y[n])}{F(x[n])} \right) \quad . \tag{2.17}$$

To equalize system frequency response consisting of speaker, preamp and A/D converter, a measurement microphone has been placed at the measurement location. The Fourier transform of the recorded impulse response $m_{Calibrate}[n]$ can then be used to filter the microphone frequency responses and thereby equalize the measurement system:

$$m_{equalized}[\varphi_i, n] = F^{-1}\left(\frac{F(m[\varphi_i, n])}{F(m_{Calibrate}[n])} \right) \quad . \tag{2.18}$$

The measurement of the speaker, a *JBL SRX-712M* stage monitor, was carried out beforehand in a similar way [LU10]: The sound radiated by the speaker was captured by a surrounding circular microphone array.

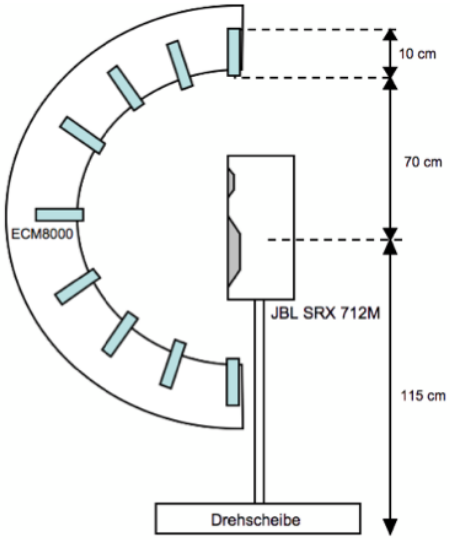

Fig. 2.7.: [LU10] Setup for the speaker impulse response measurement

Post processing

To reduce the influence of unavoidable reflections in the measured data, the impulse responses were windowed with a half *Hann* window with the length N=250 samples, which corresponds to a sound path of 1.94m. Consequently, all reflections arriving at the microphone with a longer propagation path are eliminated.

Another common problem when placing the microphone on a rotary plate, is a shift of the acoustical center, when the capsule of the microphone is due to the rotation not always placed at the exact same distance to the loudspeaker. Consequently, a time shift between the peaks of the impulse responses can be observed. Therefore, the off-axis responses have been shifted by Δn samples according to the maximum of their cross-correlation R_{xx} with the on-axis response:

(2.19) $$\Delta n = arg_{max}(R_{xx}(m[\varphi_i, n], m[0°, n]))$$

[Fig. 2.8] shows a set of impulse responses before and after the time delay correction.

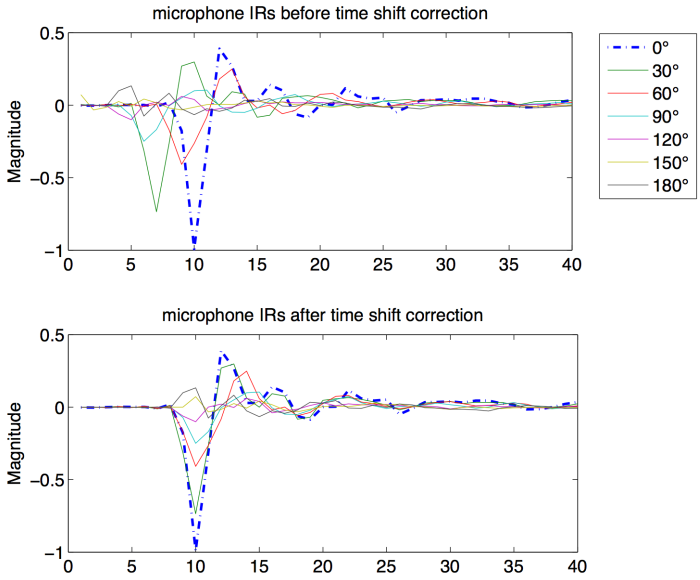

Fig. 2.8.: Microphone impulse responses before and after the time shift correction

2.4. Interpolation of directivity patterns

To achieve an accurate representation of the measured impulse responses, the measured data has to be interpolated in an appropriate way. [Zot08] proposed a strategy of representing three-dimensional radiation patterns by interpolating with weighted spherical harmonic base functions. The radiation patterns in this work are assumed to be rotationally symmetric without making large errors, which facilitates verification and keeps the demonstrations simple. Therefore, the two-dimensional equivalent of the spherical harmonics, the circular harmonic basis functions, have been used for interpolation.

By applying a Fourier transform to the measured impulse responses, the complex values are obtained for every frequency bin and every measured angle, which can be given in magnitude and phase. For a distinct frequency bin, the values p at the M angles φ can be written in a vector **p**:

(2.20) $$\boldsymbol{p}=[\,p(\varphi_1), p(\varphi_2), \ldots, p(\varphi_M)]^T \quad .$$

The circular harmonic basis functions (CHBF) of the order N are defined as a series 2N+1 of trigonometric functions depending on the angle φ:

(2.21) $$\boldsymbol{k}=[\sin(N\cdot\varphi), \sin((N-1)\cdot\varphi), \ldots, \sin(\varphi), 1, \cos(\varphi), \cos(2\cdot\varphi), \ldots, \cos(N\cdot\varphi)] \quad .$$

The underlying idea of the interpolation method is, that every polar pattern or every function depending on the angle φ can be decomposed into circular harmonic basis functions. Hence, the measured data at discrete angles, can be represented as a set of CHBFs and coefficients.

Since the CHBFs can be evaluated at every angle, values at angles between the measured points can be interpolated. In mathematical terms, the vector $\mathbf{p}_\mathbf{r}$ can be decomposed into a coefficient vector **c** and a matrix **K** containing the circular harmonic basis functions at the measured angles φ_i:

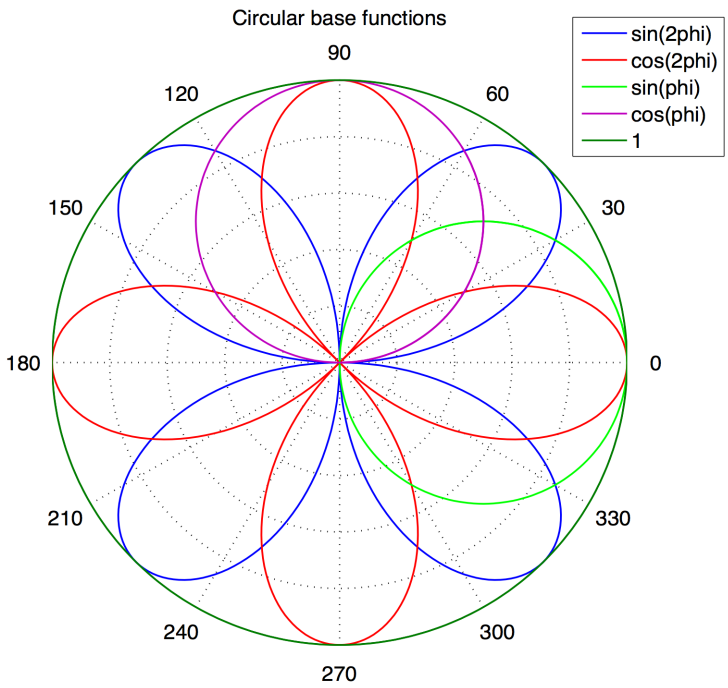

Fig.2.9: Polar representation of circular harmonic basis functions for N=2

(2.22) $$\boldsymbol{p} = \boldsymbol{K} \cdot \boldsymbol{c} \quad \text{with} \quad \boldsymbol{c} = [c_{1,\dots}, c_{(2\cdot(N+1))}]^T \quad \text{and} \quad \boldsymbol{K} = \begin{bmatrix} \boldsymbol{k}(\varphi_0) \\ \dots \\ \boldsymbol{k}(\varphi_M) \end{bmatrix} .$$

Since the CHBFs and the measured data is known, the coefficients can be obtained by inverting the matrix **K** and multiplying with **p**. There is only an exact solution, respectively the matrix **K** is invertible, if the number of measurement point M equals 2N+1. For the interpolation of the directivity patterns, the CHBF order N was chosen in a way, that this condition was fulfilled, hence the measured points were represented accurately and the space within them interpolated [Fig. 2.10].

(2.23) $$\boldsymbol{c} = \boldsymbol{K}^{-1} \cdot \boldsymbol{p} \quad .$$

As described in [Pom08], when the matrix **K** is not quadratic, a solution can be approximated by applying the Moore-Penrose pseudo inverse, which corresponds to a least square approximation:

(2.24) $$\boldsymbol{c} = pinv(\boldsymbol{K}) \cdot \boldsymbol{p} \quad .$$

Once the coefficient vector c is known, the value of the sound pressure p can be interpolated for arbitrary angles φ by multiplying the phase-dependent CBF-vector with the coefficient vector:

(2.25) $$\boldsymbol{p}(\varphi) = \boldsymbol{c} \cdot \boldsymbol{k}(\varphi) \quad .$$

The procedure is being repeated for every frequency bin and as a result, the frequency responses of the microphone M(f, φ) and the loudspeaker S(f, φ) can be calculated for arbitrary angles φ. Alternatively, the described procedure can also be applied in the time domain, which leads to angle-dependent impulse responses m(t, φ) and s(t, φ). In case of this simulation (*Chapter 2.11*), it turned out to be computationally more reasonable to interpolate the time domain response.

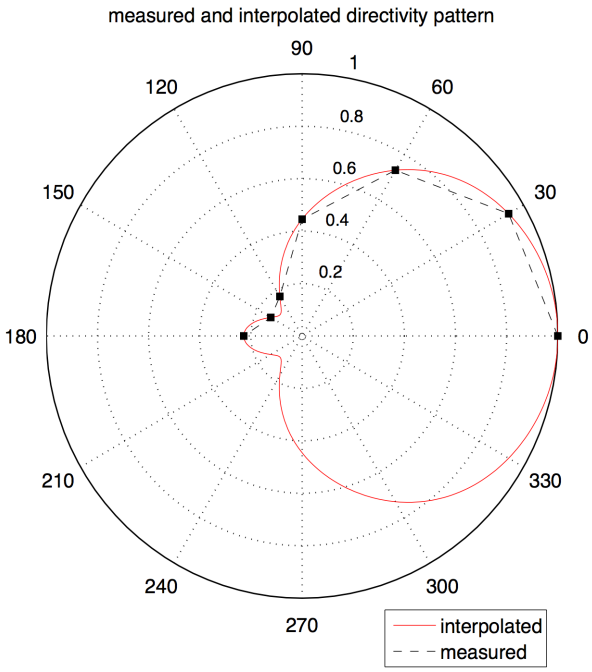

Fig. 2.10: measured and interpolated microphone directivity pattern

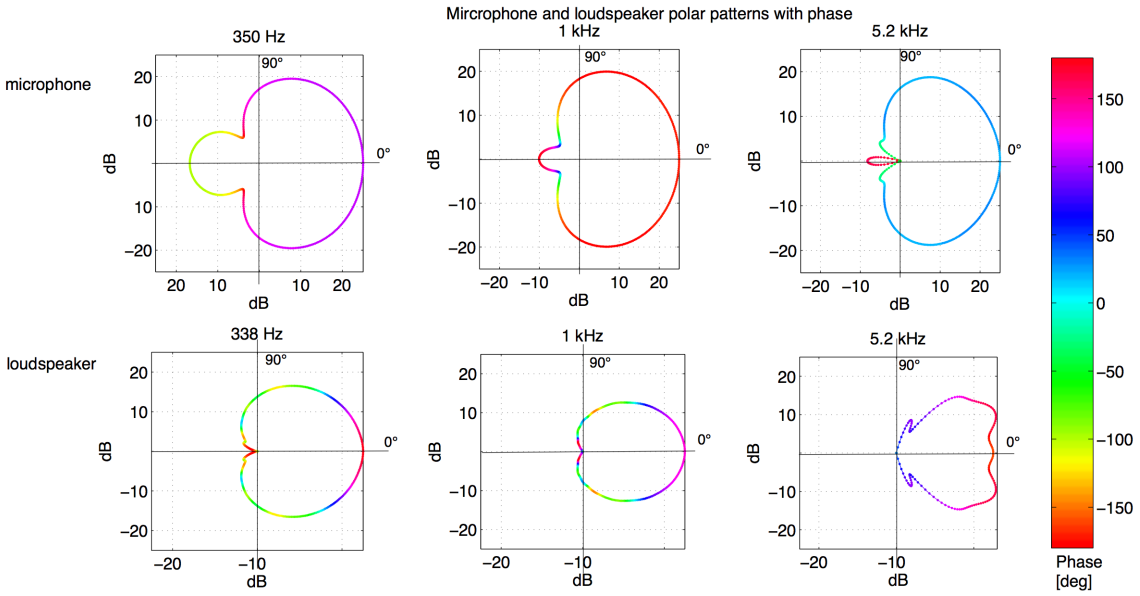

Fig. 2.11: interpolated polar patterns for microphone and loudspeaker at various frequencies

[Fig. 2.11] shows microphone polar patterns at different frequencies. It becomes obvious that the directivity characteristics show significant frequency dependent

behavior. The directivity becomes stronger with increasing frequency and the rear lobe of the microphone is less pronounced at higher frequencies.

2.5. The importance of phase information in directivity patterns

Usually manufacturers of microphones and loudspeakers provide the user with magnitude frequency responses and polar patterns. Less attention on the other hand has been payed to the phase information of such devices. Back in 1971 [Sch71] already pointed out the importance of the phase response data for the accurate representation of microphone characteristics. Although it was back then a lot more complex to measure the phase response, [Sch71] showed that the phase response for directional microphones is angle dependent and that the phase shifts are significantly higher than for omnidirectional microphones. With the possibilities of computer based Fourier transforms, the measurement of the phase response became a lot simpler. [ABFM00] showed the importance of phase data for the summation of various loudspeaker signals with different phase responses. The impact of the radiation phase data on this simulation method will be further investigated in Chapter 3 by comparing simulation results using complex frequency responses with those when only the absolute value is being considered. [Fig. 2.11] shows the phase information of microphone and loudspeaker as values of a colormap. It can be seen, that the phase changes especially between the main and the rear axis of the microphone. The speaker radiates with a constant phase for low frequencies, while at higher frequencies angle-dependent phase changes can be observed.

2.6. The mirror source principle

The mirror source principle is a method of geometric room acoustics presented by [AB78], which is often being used in room acoustic simulations, e.g. [Kre01], to model early reflections in small, simple-shaped rooms [Fig. 2.12]. The sound reflected at a rigid wall is modelled by placing image sources S_i at the same distance to the respective

wall as the original sound source S_0. The sound at the receiver position R consists of the summation of the direct sound and the sound of the image sources. To model reflections of a higher order, the mirror sources have to be mirrored again at every other wall.

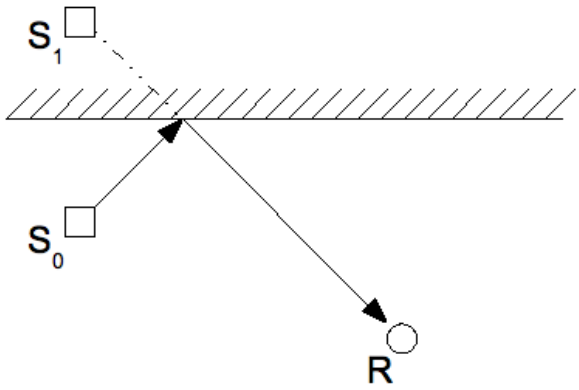

Fig. 2.12: mirror source principle

In the case of right-angled cornes, as assumed in this simulation, a special case is present: As in [Cre78] explained in further detail, every incoming sound wave leaves the corner after being reflected twice, which results in only one second order mirror source in every corner. In other terms, only one of the two second order mirror sources at the same position, is visible. In this case the angle bisector of the corner is the border which determines which of the two sources is visible.

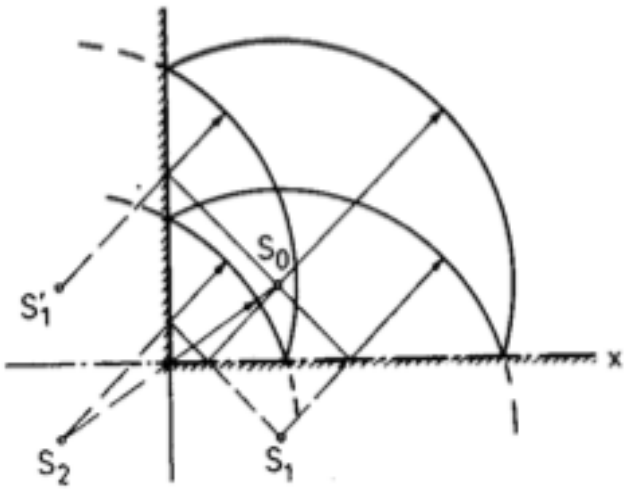

Fig. 2.13: [Cre78], Chapter 2, Reflection at a right-angled corner

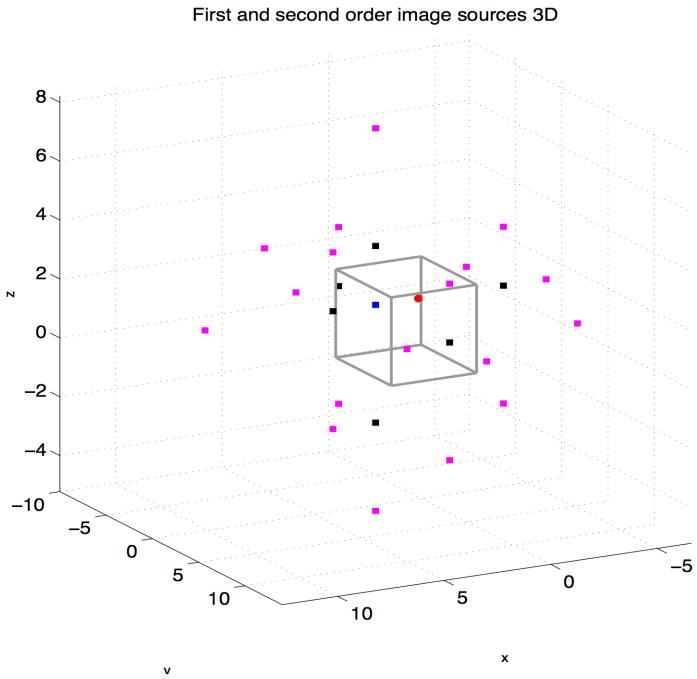

Fig. 2.14: simulated image sources of first and second order

In this work, the mirror source principle was extended in a way, that also the directivity of the source is being considered: When the sound source is not omnidirectional, also the shape of the directivity has to be mirrored at the respective wall, resulting in a mirroring of the directivity pattern at the corresponding axis.

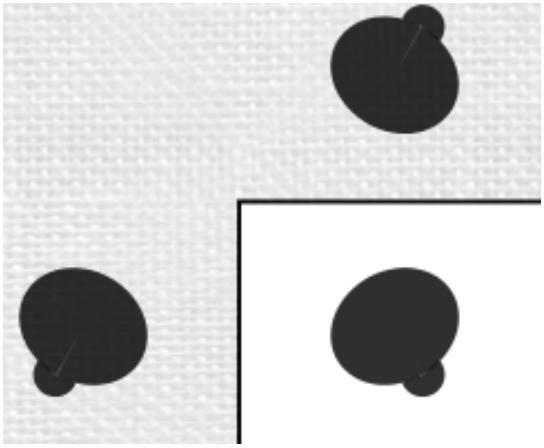
Fig. 2.15: schematic illustration of the mirroring of directivity patterns

Once the positions of source, receiver and mirror sources are known, the angle at which the sound leaves the (image) source α as well as the angle at which the sound reaches the receiver β can be obtained using simple geometrical methods.

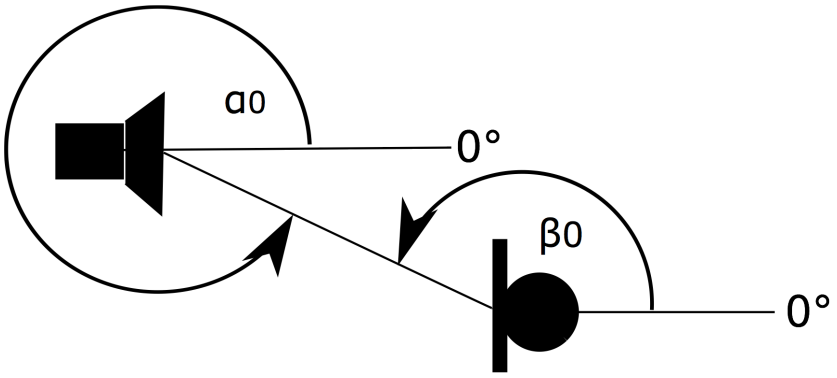

Fig. 2.16: angles for incoming and outgoing sound

Thereby, the corresponding angle-dependent frequency responses of microphone and loudspeaker, can be obtained. In this work, an angle of 0 degrees always corresponds to the positive x axis. For the two-dimensional case, with the microphone coordinates (mx, my) and the source coordinates (sx_i, sy_i), the angles α_i of the outgoing sound follow as:

(2.26) $$\alpha_i = \arctan\left(\frac{my - sy_i}{mx - sx_i}\right) \quad .$$

Correspondingly, the angles β_i of the incoming sound can be calculated as:

(2.27) $$\beta_i = arctan2\left(\frac{y_i - my}{sx_i - mx}\right) \quad .$$

Ambiguities in the angles can be resolved by observing the relation of the locations of the microphone and the loudspeaker.

For the three-dimensional case, the calculation of the angles of the incoming and outgoing sound become more complex: Under the assumption of rotation symmetry, the impulse response varies only with the axial angle, which varies between 0 and π. In this case, α_i and β_i can be determined from their unity vectors $\boldsymbol{s_e}$ and $\boldsymbol{m_e}$ and the vector $\boldsymbol{ms}$ between them:

(2.28) $$\alpha_i = \arccos\left\langle \frac{\vec{ms}}{\|\vec{ms}\|} \cdot \vec{s}_e \right\rangle \quad ,$$

(2.29) $$\beta_i = \arccos\left\langle \frac{\vec{ms}}{\|\vec{ms}\|} \cdot \vec{m}_e \right\rangle \quad .$$

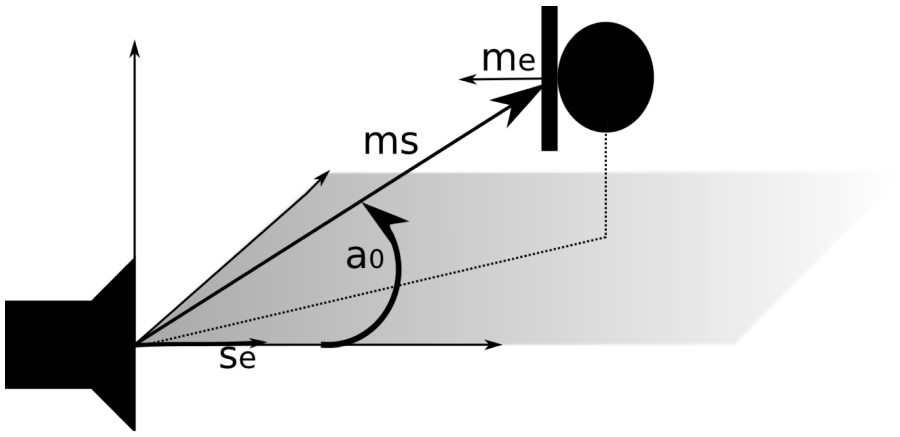

Fig. 2.17: angle for the outgoing sound in 3D

The mirror source principle seems to be appropriate for investigating the feedback behavior since it describes the early - and consequently strongest - reflections of the sound radiated by the source, which reach the microphone and therefore contribute most likely to the occurrence of acoustic feedbacks. The drawback of the this method is, however that it does not include the modeling of room modes which depend on the geometrics of the room. The frequency interval, in which standing waves occur becomes smaller with increasing frequency and through spectral density of the room modes, they loose their significance. The *Schroeder* frequency provides a good boundary value for this issue [MM04]:

(2.30) $$f_s = 2000 \cdot \sqrt{\frac{T}{V}} \qquad T... \ reverberation\,time \qquad V... \ room\,volume \quad .$$

For example, in a room of the dimensions of 3m x 6m x 2.5m with a reverberation time of 1.5 s, the *Schroeder* frequency is f_s = 365 Hz. For frequencies above f_s, the image source model as well as other geometrical or statistical room models give a sufficient description of the room acoustic behavior. The behavior of the frequency range below f_s on the other hand, is dominated by room modes and can be described best by using wave theory. Furthermore, the application of the image source model requires the

dimensions of the absorption surfaces to be large and wall structures to be small compared to the wave length.

2.7. Magnitude attenuation and time delay

With knowledge of the distance between the sources and the receiver, the magnitude attenuation due to the propagation in air and the time delay of the reflected waves can be calculated. According to the *distance law*, the magnitude of a sound wave decreases with the distance d from the source by 1/d, which always holds for omnidirectional sources, and is true for the far-field of directional sources.

The time delay Δt of the arrival of the sound can be calculated from the sonic speed v=343 m/s and the distance:

(2.31) $$\Delta t = \frac{d}{c} \quad .$$

When applying the mirror source principle, the distance between an image source and the receiver corresponds to the length of the sound path of the respective reflected wave and can therefore be used when calculating the amplitude attenuation and the time delay.

Consequently, the delayed and attenuated impulse response of the loudspeaker s(t) at the receiver position $s_{rec}(t)$ follows from the above to:

(2.32) $$s_{rec}(t) = \frac{1}{d} \cdot s(t + \Delta t)$$

2.8. Reflection on surfaces

In case of non-rigid walls, a certain amount of the energy - described by the absorption

coefficient α - of the sound wave is being absorbed during the reflection at the wall. An absorption coefficient α=1 corresponds to full absorption, while α=0 represents a rigid wall. In general, the absorption of surface materials is frequency dependent. Appendix [A] shows the absorption coefficients for the materials used in the simulation in third octave bands from [Gol].

With the values for α provided in Appendix [A], an impulse response for the reflection on a surface can be constructed from the absorption coefficients. The magnitude values at octave band frequencies are given by:

(2.33) $$A(f_{oct}) = \sqrt{1-\alpha(f_{oct})^2} \quad .$$

These known magnitude values can be multiplied with *Hann* windows to obtain an interpolated frequency response. The weighted windows should be arranged in a way that the falling slope approaches exactly the next octave frequency, as schematically shown in [Fig. 2.18]. The resulting frequency response is the sum of the weighted window functions surrounding.

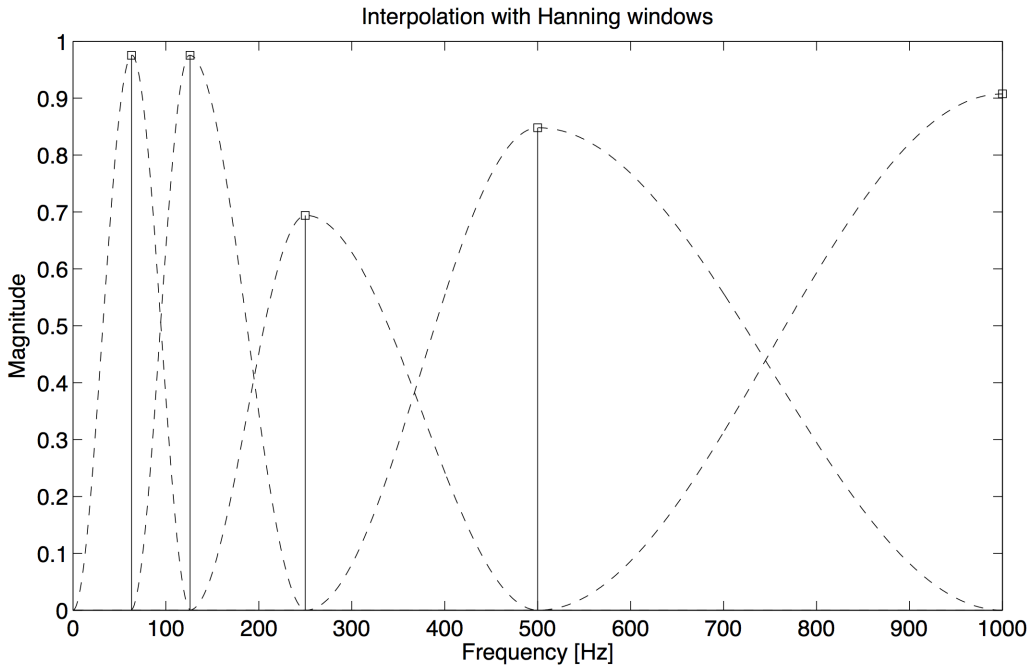

Fig. 2.18: frequency response construction using Hann windows

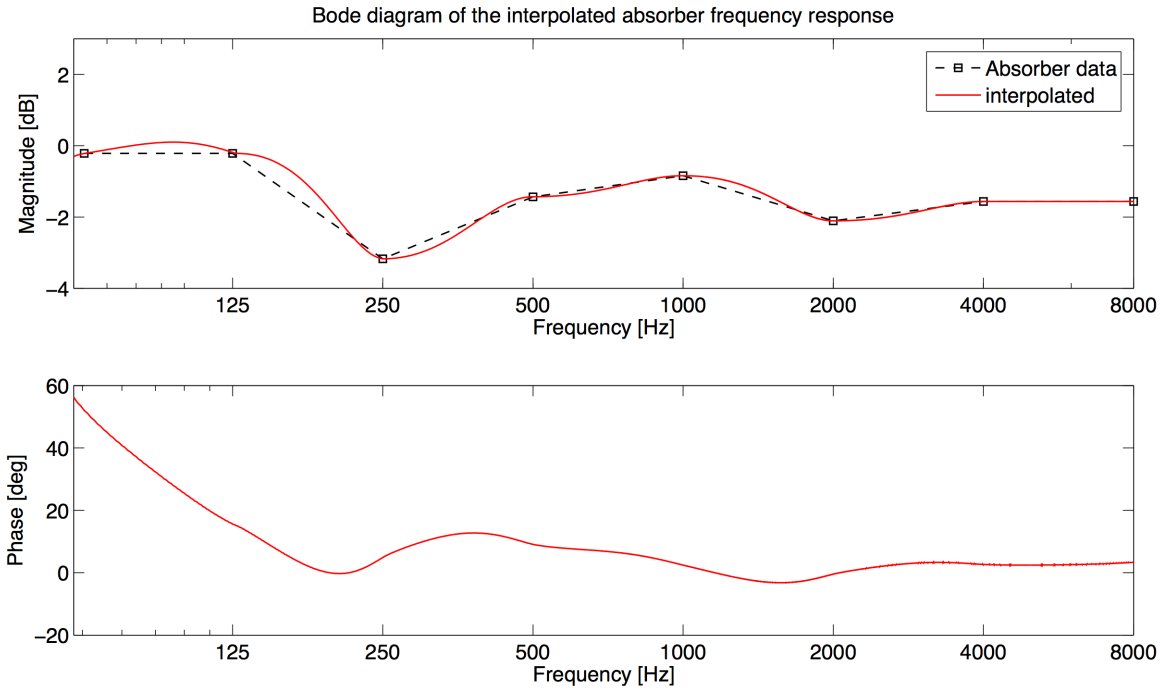

Fig. 2.19: Interpolated bode diagram of an absorber frequency response

Since there is no phase information present in the absorber data, a minimum-phase response is being constructed, as discussed in [PL]:

Assuming the absorber impulse response a[n] to be a minimum-phase sequence, its *cepstrum* $\boldsymbol{A}[n]$ is causal, i.e. $\boldsymbol{A}[n]=0$ for $n<0$. Consequently, a minimum-phase sequence can be obtained from an arbitrary sequence, by dropping the non-causal part of its *cepstrum*. Let A(f) be the frequency response of the absorber as described above, the *cepstrum* can be calculated by finding the logarithm of the spectrum and performing the inverse Fourier transform:

(2.34) $$\boldsymbol{A}[n]=F^{-1}\{\log[A(f)]\} \quad .$$

The non-causal part can be excluded, by multiplying with a rectangular window w and weighting the first and the last coefficient:

(2.35) $$\boldsymbol{A}_{causal}[n]=\boldsymbol{A}[n]\cdot w[n], \qquad w[n]=\begin{bmatrix} 1 \; for \; n>0 \\ 2 \; for \; n=0 \;\wedge\; n=N \\ 0 \; for \; n\leq 0 \end{bmatrix} \quad .$$

The minimum-phase absorber impulse response can finally be obtained by transforming the exponential spectrum back to the time domain:

$$a_{causal}[n] = F^{-1}\{e^{F\{A_{causal}[n]\}}\} \quad . \tag{2.36}$$

In this work, the simplification has been made, that the absorption coefficient α is independent of the angle of incidence θ, which is not the case in reality. Usually, absorber data refers to the averaged value over all angles of incidence, as described in [MM04]:

$$\alpha_{averaged} = 2 \cdot \int_0^{\pi/2} \alpha(\theta) \cdot \sin(\theta) \cdot \cos(\theta)\, d\theta \quad . \tag{2.37}$$

2.9. Diffuse field model

Since the image source model only covers the early reflections, a statistical approach has been used to model the late reverberation. While the amplitude of the direct sound decreases with the distance d according to the *distance law*, the reverberant field can be statistically taken into account as constant. At the so-called *critical distance* d_C, the direct and the reverberant sound field have the same level. The *critical distance* can be calculated from the room volume V, the reverberation time T_{60} and the directivity factor γ:

$$d_C \approx 0.057 \cdot \sqrt{\gamma} \cdot \sqrt{\frac{V}{T_{60}}} \quad . \tag{2.38}$$

The reverberant time T_{60} is calculated with the *Sabine* equation, where S is the room surface and α the average absorption coefficient:

$$T_{60} \approx 0.1611 \mathrm{m}^{-1} \cdot \frac{V}{S \cdot \alpha} \quad . \tag{2.39}$$

Combining the two equations and simplifying leads to:

(2.40) $$d_C = 0.057 \cdot \sqrt{\gamma} \cdot \sqrt{(S \cdot \alpha)} \quad .$$

As mentioned before, microphones have angle-dependent frequency responses, hence the receiver will capture the diffuse reverberations with a different frequency response as the direct sound arriving on the main axis. The statistical approach is based on the assumption that the energy of the diffuse reflections is distributed equally in the room. The *diffuse field response* corresponds to the frequency dependent *Random Energy Efficiency (REE)* and describes the frequency characteristics of a microphone under these circumstances and can be derived from the angle-dependent frequency responses under the assumption of symmetrical directivity patterns as shown in [Sch71]:

(2.41) $$M_{diffuse}(f) = 0.5 \cdot \int_0^{\pi} \left(\frac{M(f,\varphi)}{M(f,\varphi=0)} \right)^2 \cdot \sin(\varphi)\, d\varphi \quad .$$

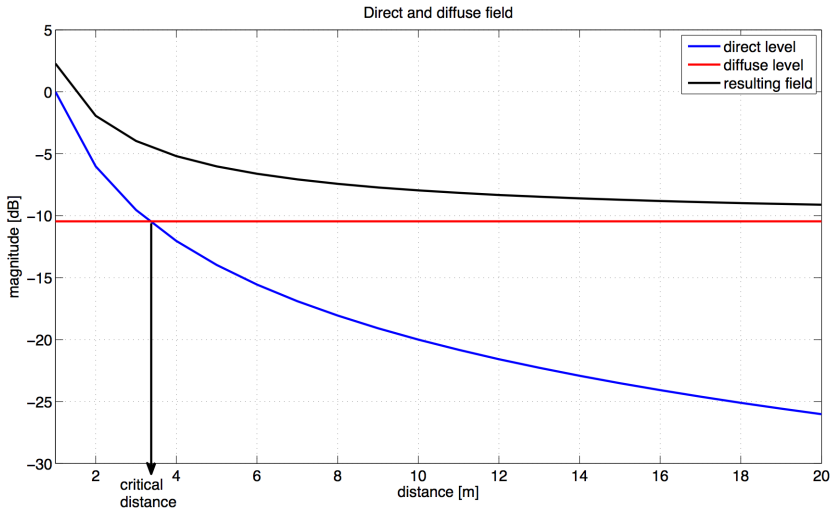

Fig. 2.20: critical distance, direct field (blue), reverberant field (red) and overall sound field (black)

Applying *Simpson's rule*, the equation can be simplified, where b is the interval between the measured angles and N the number of measurement samples.

(2.42) $$x(\varphi) = 0.5 \cdot \left(\frac{M(f,\varphi)}{M(f,\varphi=0)} \right)^2 \cdot \sin(\varphi) \quad ,$$

(2.43) $$M_{diffuse}(f) = b/3 \cdot [x(0) + 4x(\varphi_1) + 2x(\varphi_2) + 4x(\varphi_3) + \ldots + 2x(\varphi_{N-2}) + 4x(\varphi_{N-1}) + x(\varphi_N)] \quad .$$

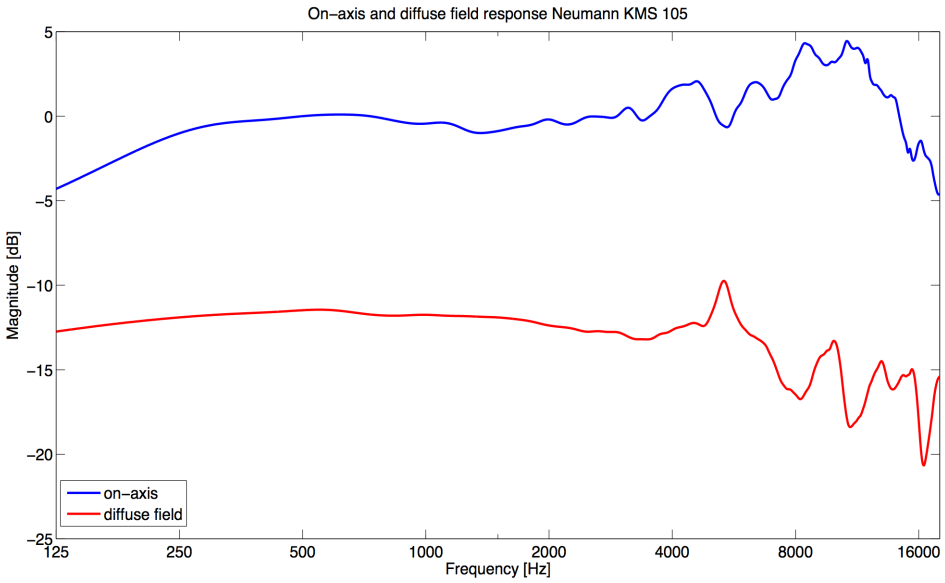

Fig. 2.21: free field (on-axis) response (red) vs. diffuse field response (blue)

[Fig. 2.21] shows the resulting diffuse field response of a super-cardioid condenser microphone in comparison with its free field (main axis) response. Since there is no concrete phase information about the diffuse field, it can be considered with zero or random phase. In this simulation approach, a zero-phase diffuse field was implemented. This scenario can be regarded as the worst case.

The same process can be applied to derive the directivity factor γ of the loudspeaker from the angle dependent source frequency responses. The directivity factor is the inverse REE and therefore frequency dependent. In this simulation, an average value has been used:

(2.44) $$\gamma = \frac{1}{\overline{REE}(f)} \quad .$$

With the critical distance d_C, the transfer function for the diffuse field can be calculated as:

(2.45) $$L_d(f) = \frac{1}{d_C} \cdot M_{diffuse}(f) \quad .$$

2.10. Loop transfer function

The aim is now to define a loop transfer function L(f), that describes the feedback path between loudspeaker and microphone including their frequency responses, early reflections, absorption on wall surfaces and the diffuse field for distinct room characteristics and microphone and source positions.

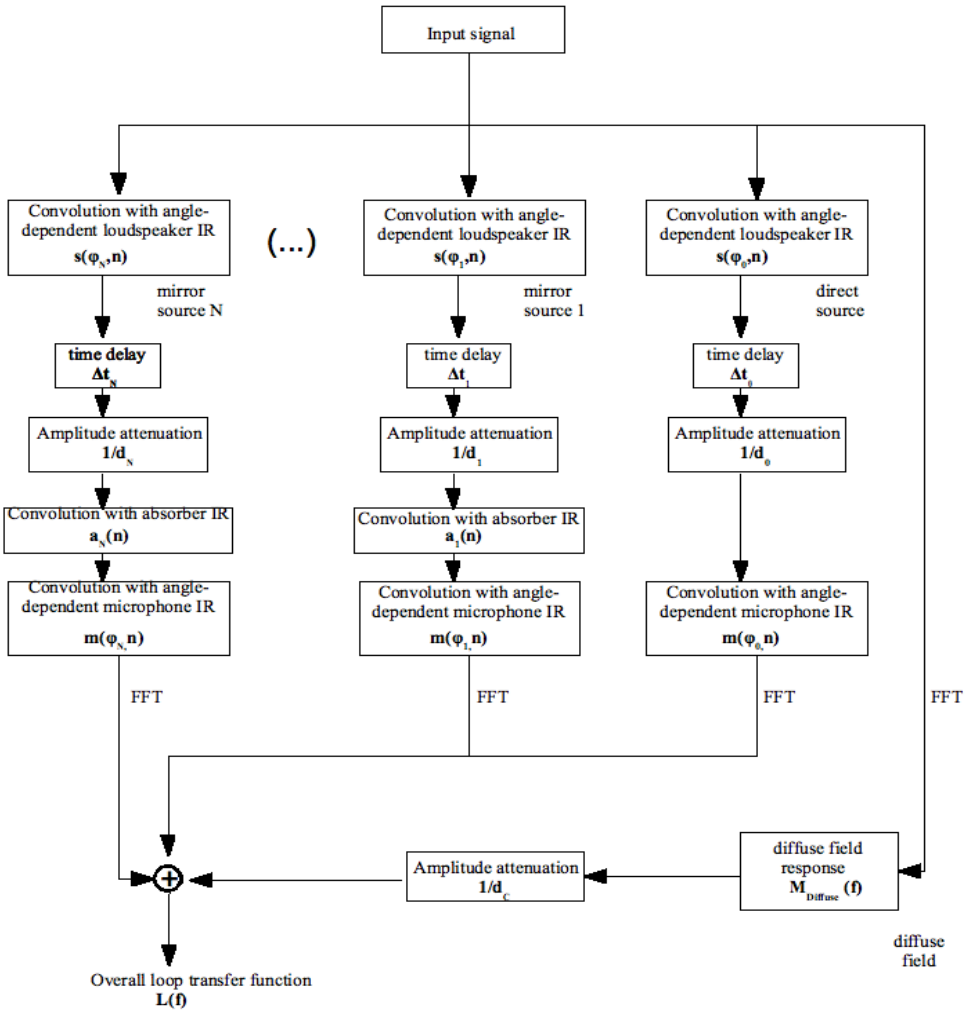

Fig. 2.22: signal flow for the calculation of the loop transfer function

[Fig. 2.22] shows the signal flow of the feedback loop. For computational reasons, some operations are processed in the time domain (lower-case characters) and others in the frequency domain (capital letters).

angle-dependent loudspeaker impulse response	**s[φ,n]**
angle-dependent microphone impulse response	**m[φ,n]**
time delay	**Δt**
distance between source and receiver	**d**
absorber impulse response	**a[n]**
diffuse field response of microphone	**D(f)**
critical distance	**d_C**
number of image sources	**N**
image source index	**i**
time index	**n**

Accordingly, the overall loop transfer function L(f) can be calculated as the sum of the transfer function of the direct path $L_0(f)$, the sound paths of the mirror sources $L_i(f)$ and the diffuse field transfer function $L_D(f)$:

(2.46) $$L_o(f) = F\{\frac{1}{d_0}\cdot(s[\varphi_{0,}n+\Delta t_0]*m[\varphi_{0,}n])\} \quad ,$$

(2.47) $$L_i(f) = F\{\frac{1}{d_i}\cdot(((s[\varphi,n+\Delta t_i]*a_i[n])*m[\varphi_i,n]))\} \quad ,$$

(2.48) $$L_D(f) = \frac{1}{d_c}\cdot M_{diffuse}(f) \quad ,$$

(2.49) $$L(f) = L_0(f)+L_1(f)+...+L_N(f)+L_d(f) \quad .$$

If only the magnitude criterion is considered, the MSG in dB is the negative logarithmic value of the maximum of the loop transfer function:

(2.50) $$MSG \approx -20\cdot\log(max|L(f)|) \quad .$$

The impulse responses m(Φ,n) and s(Φ,n) have been normalized in a way, that their maximum value – considering all angles – was set to 1. This means that in the proposed model, neither the microphone nor the loudspeaker itself perform any amplification, i.e. their internal gain factors were decoupled and are part of the overall, scalar system gain factor g. In reality of course, microphone and loudspeaker have a distinct transmission factor.

2.11. The proximity effect

A common phenomenon of directional microphones is the dependence of the frequency response from the source distance. In particular, an enhancement of low frequencies below 1kHz takes place for small microphone to source spacings. In literature [Mar06] various explanations can be found for this effect. The most consistent appears to be the location dependency on the pressure gradient of the sound source [Lit06].

For directional microphones, the membrane is accesible for the sound pressure from both sides. Consequently, they transmit the pressure gradient, determined by the angle-dependent path difference of the incoming wave between both sides of the microphone. By incorporating an adjusted delay line device, a specific directional behavior can be obtained.

The pressure gradient can be understood as the spherical derivative of the sound pressure. The pressure p of a spherical wave with the angular frequency ω, the wave number k and the magnitude A can be described at the distance r and the time t as:

(2.51) $$p(r,t)=\frac{A}{r}\cdot e^{j(\omega\cdot t-k\cdot r)} \quad .$$

The pressure gradient can be obtained by differentiating the distance r:

(2.52) $$\nabla p=\frac{\partial}{\partial r}\cdot\left(\frac{A}{r}\cdot \mathrm{e}^{\omega\cdot t-k\cdot r}\right) \quad ,$$

(2.53) $$\nabla p = \frac{-A}{r} \cdot \left(\frac{1}{r} + jk\right) \cdot \mathrm{e}^{(j(\omega \cdot t - k \cdot r))} \quad .$$

In the far-field, the radius r fullfils the condition:

(2.54) $$\frac{1}{r} \ll k \quad .$$

Consequently, the approximation can be made, that the pressure gradient increases linearly with the radius r:

(2.55) $$\nabla p_{\text{far-field}} \sim \frac{1}{r} \quad .$$

In the near-field, both terms of equation (2.53) are dominant and the relation is quadratic:

(2.56) $$\nabla p_{\text{near-field}} \sim \frac{1}{r^2} \quad .$$

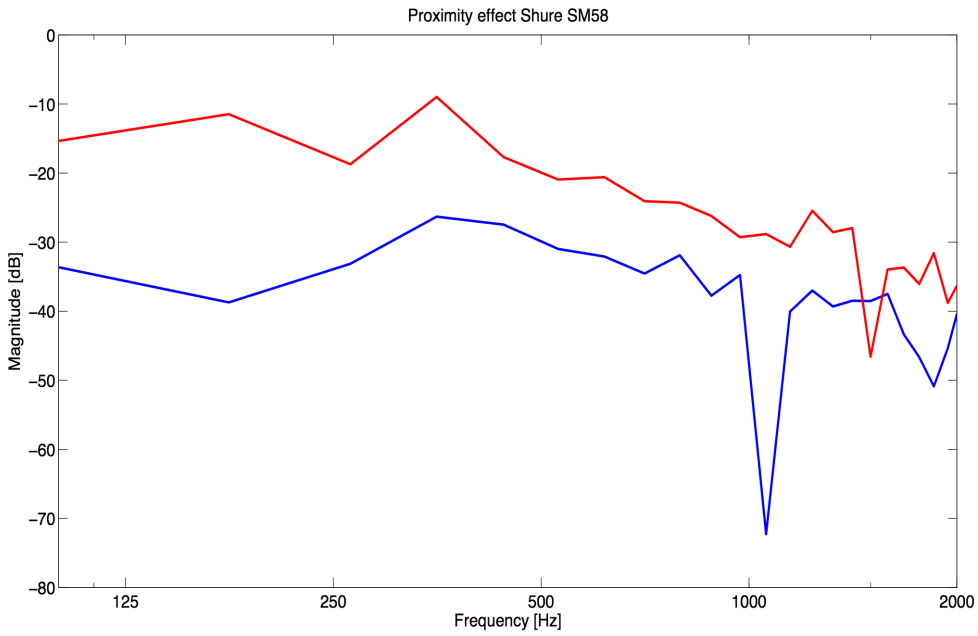

Fig. 2.23: Proximity effect of the Shure SM58

Since, the radius of the near-field is greater for low frequencies, an enhancement of the low frequency area, known as the proximity effect, takes place. In [Fig. 2.23] the proximity effect of the dynamic Shure SM58 microphone can be observed.

To consider the influence of the proximity effect on the feedback behavior, the bass enhancement can be modeled as an additional filter applied to the input system. The resulting transfer function of the overall feedback network is then modified to:

(2.57) $$H = \frac{r(t)}{s(t)} = \frac{g \cdot P}{1 - L \cdot g} \quad .$$

Although the gain before instability is still limited by the loop transfer function, with the same gain value, a higher level for low frequency can be obtained at the output. The influence of the proximity effect will be further investigated in Chapter 3.

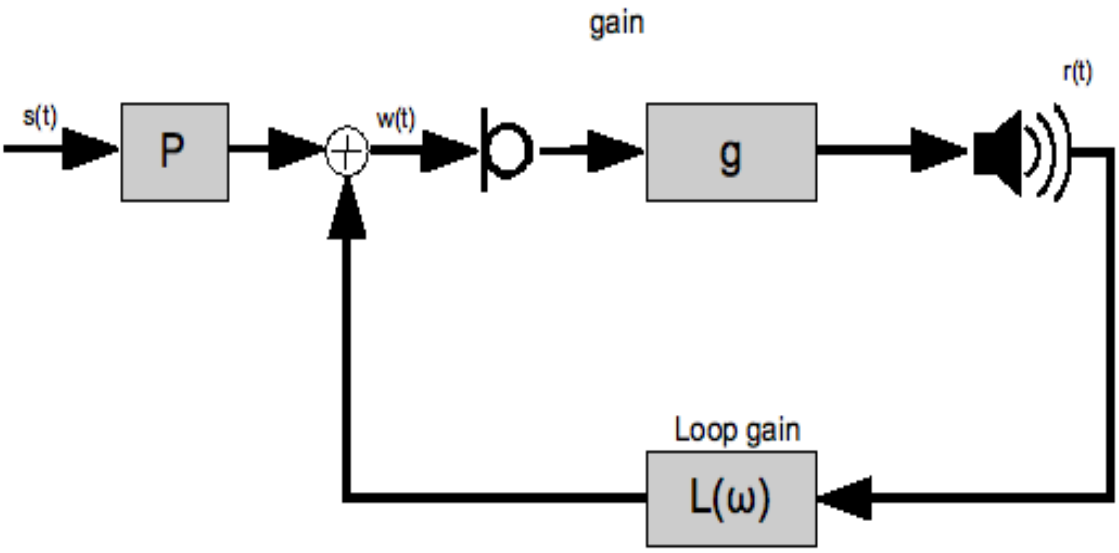

Fig. 2.24: Proximity effect in the feedback network

2.12. Implementation

For the realization in *MATLAB*, a graphical user interface has been developed, where the position and orientation of microphone and loudspeaker, room dimensions, microphone type and absorption parameters can be modified. The output is the maximum stable gain, the peak frequency, the loop transfer function and a graphical representation of the simulated room including source, receiver and image sources.

Furthermore, a real-time version has been implemented in *PureData*, where a speech signal is convolved with the overall transfer function. This simulation is limited to a two-dimensional fixed room with first order image sources. Again, position and orientation of microphone and loudspeaker can be modified and the influence of the applied gain factor signal is made audible in real-time.

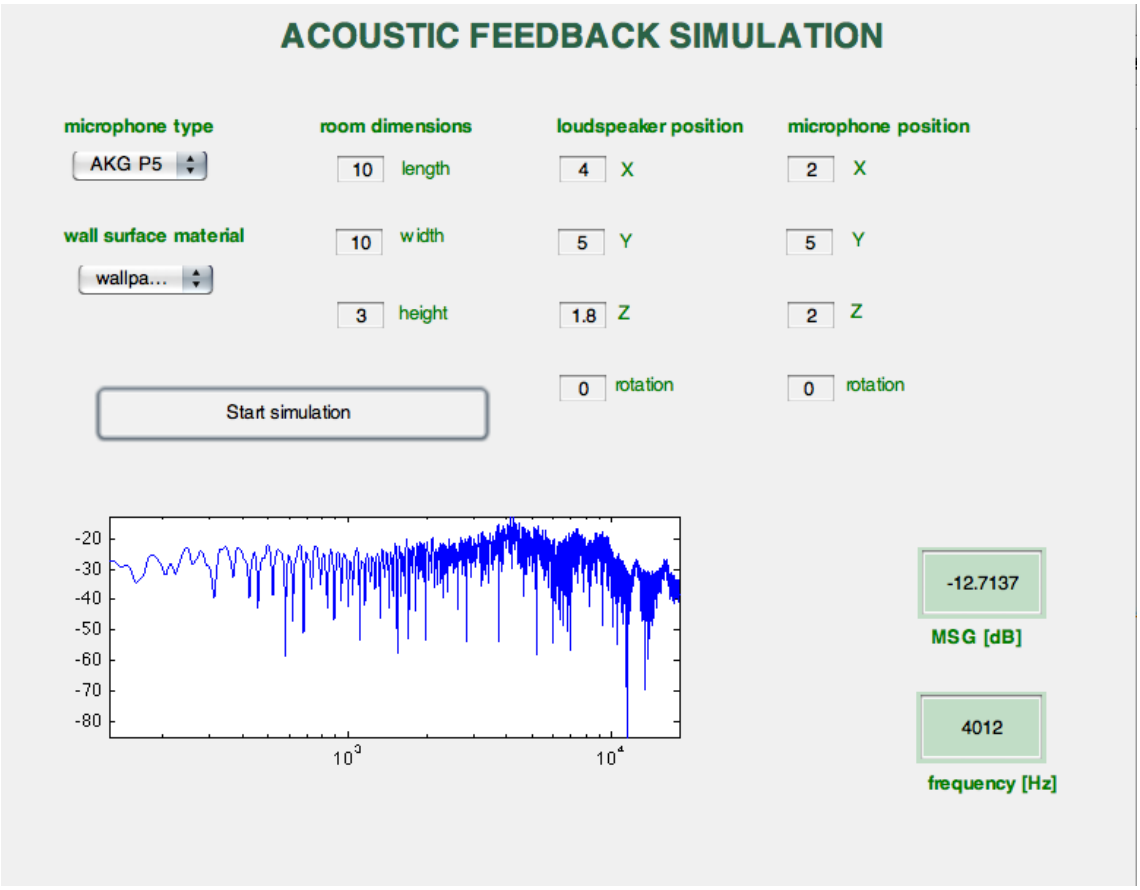

Fig. 2.25: Screenshot MATLAB graphical user interface

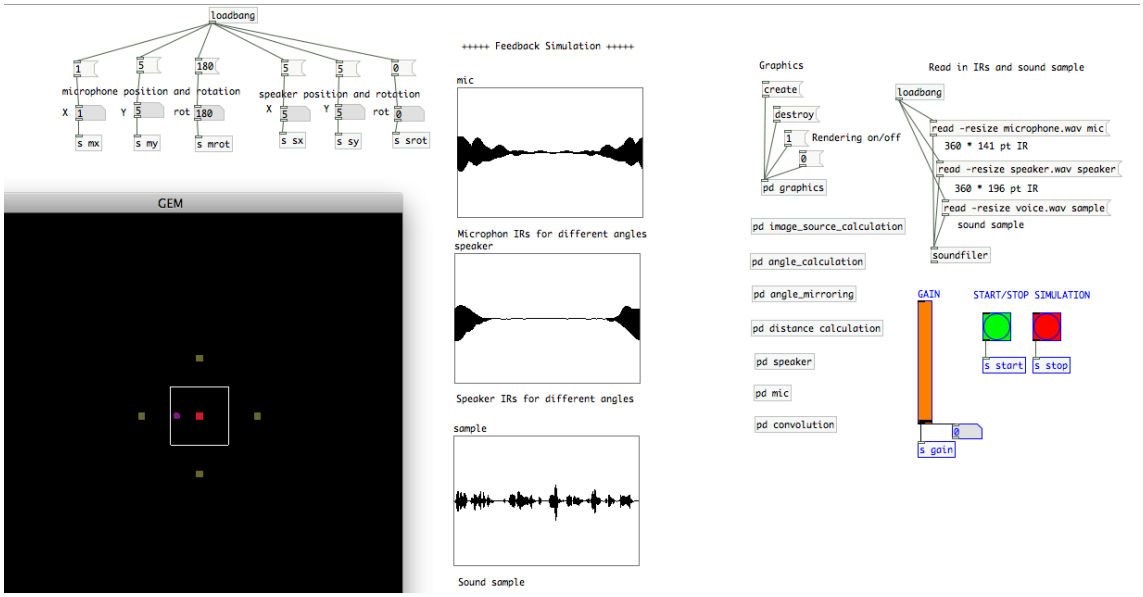

Fig. 2.26: Screenshot *PureData* patch

Chapter 3

SIMULATION RESULTS

3.1. Idealized setup

Let us first consider a microphone-loudspeaker system in an anechoic chamber, where both microphone and loudspeaker have flat, zero phase, angle independent frequency responses. In this case, the signal at the microphone simply coincides with the delayed and attenuated loudspeaker input signal [Fig. 3.1 (a)]. The frequency response of the loop transfer function L(f) is flat and the phase shows regular changes caused by the time delay.

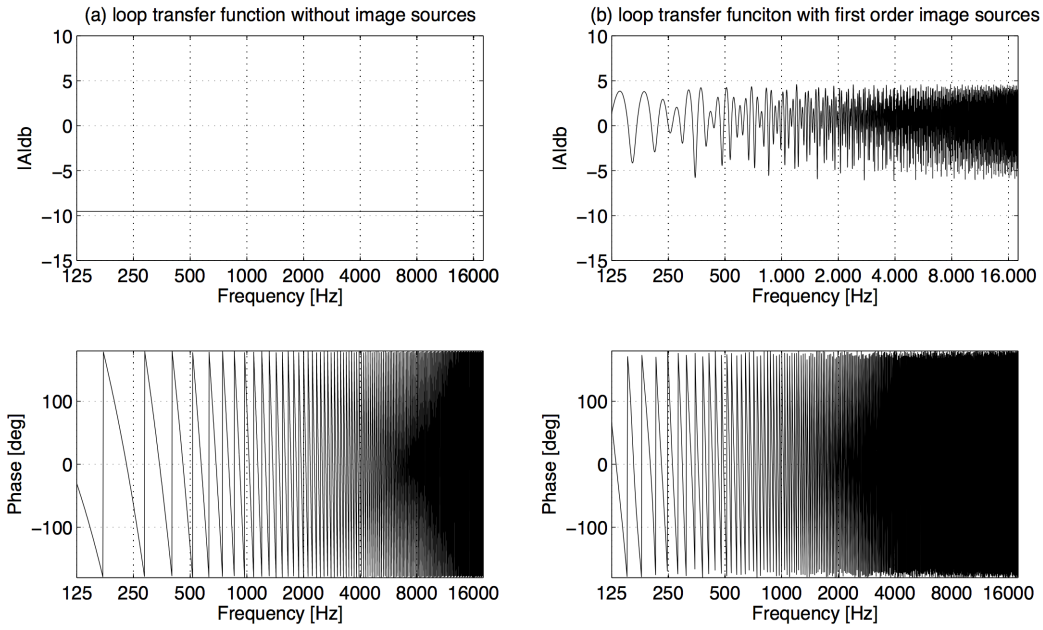

Fig. 3.1: bode diagram of the loop transfer function: (a) anechoic chamber, (b) with image sources

The simulation environment is now extended to a room with rigid walls, i.e. image sources (first order) are placed. As illustrated in the bode diagram in [Fig. 3.1 (b)], the magnitude response becomes riffled and the phase response shows faster changes and appears to be less regular over the frequency. This is due to the interference of the direct

source with the image sources, which arrive with different time delays. It becomes obvious, that even when the frequency responses of both devices are flat, the early reflections will cause a ripple in the loop transfer function. If then the gain is applied and increased, feedback will occur first at the frequency where the loop transfer function has its peak.

Let us take a closer look at the behavior of the phase response in case of an anechoic chamber. As mentioned at the beginning, the phase changes more rapidly on the frequency axis, when the distance between source and receiver is increased [Fig. 3.2 (a)] and [Fig. 3.2 (b)]. The same can be observed when the image sources are present. Especially in case of a very small distance of 1m [Fig. 3.2 (c)], the phase response has a similar envelope as the one in the anechoic chamber. This can be explained by the fact that at such a short distance the influence of the mirror sources is very low compared to the direct source. Thus, also the frequency response be smoother than at greater distances.

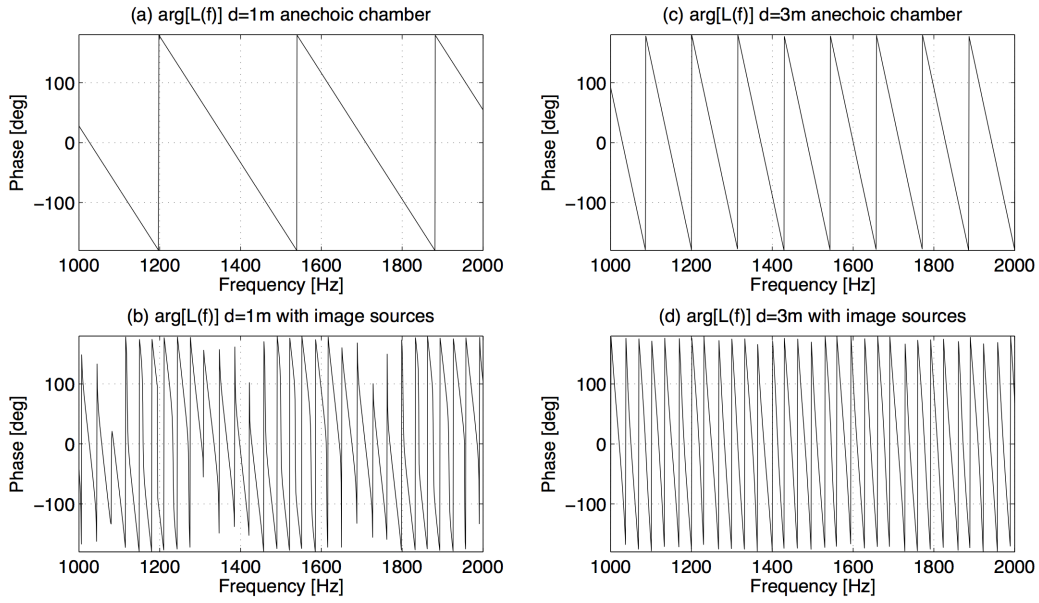

Fig. 3.2: comparison of phase responses: (a) and (b) anechoic chamber, (c) and (d) with image sources present; (a) and (c) d=1m; (b) and (d) d=3m

This observation is of importance, when discussing the consideration of the phase criterion. As mentioned before, the frequency at which the phase criterion is fulfilled is

close to the peak frequency when the phase changes more rapidly over the frequency. Hence, the magnitude criterion is a good indicator for the maximum stable gain when the distance between source and receiver is large and the error which occurs, when neglecting the phase criterion becomes bigger, when the distance is decreased. Of course, as further examples will show, the phase and magnitude responses becomes more irregular, when the angle dependent frequency and phase characteristics of microphone and loudspeaker are taken into consideration.

3.2. The closed loop and the importance of the phase criterion

To investigate the adequacy of the magnitude criterion as an estimation of the maximum stable gain, the transfer function of the overall system, the closed loop transfer function H(f), has been simulated. As expected, the peaks of the loop transfer function L(f) produce elevations in the magnitude of the closed loop transfer function, which rise with increasing system gain, as illustrated in [Fig. 3.3].

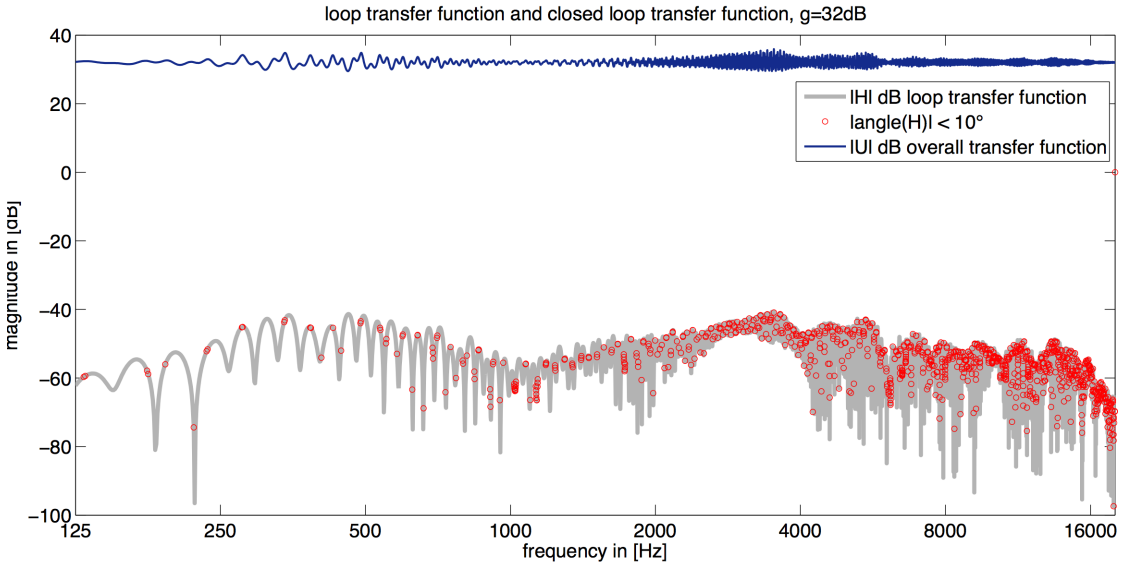

Fig. 3.3: loop and closed loop transfer function with a gain of 32dB

It is though obvious, that the loop transfer function is less smooth and shows many narrow peaks even in areas, where H(f) is has no strong riffle. This is due to the phase

of the loop transfer function: If the microphone-room-loudspeaker system produces a phase shift, a destructive interference between the feedback signal and the direct input signal occurs. This fact is taken into consideration in the phase criterion, which demands a phase shift of multiples of 2π for the incurrence of instability.

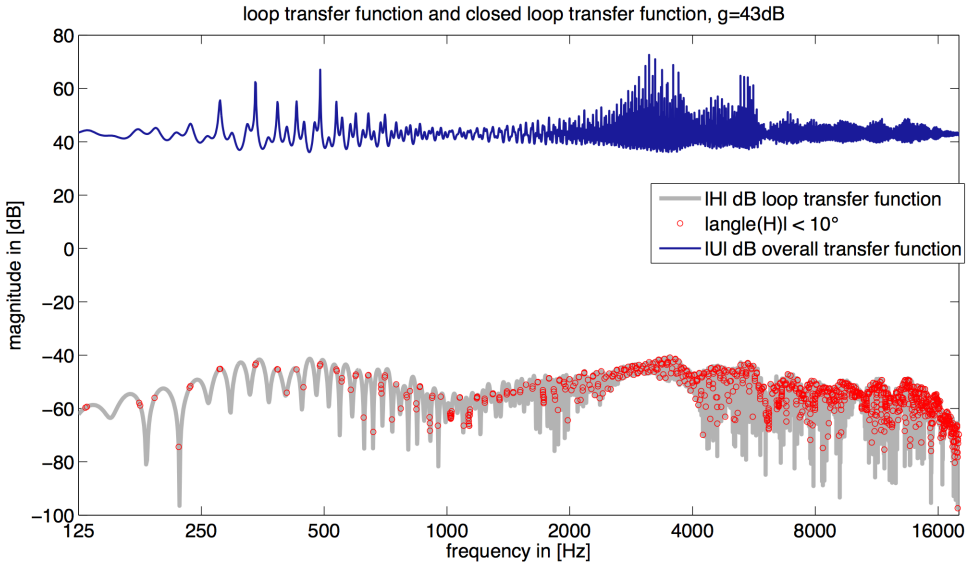

Fig. 3.4: (a) loop and closed loop transfer function with a gain of 43dB

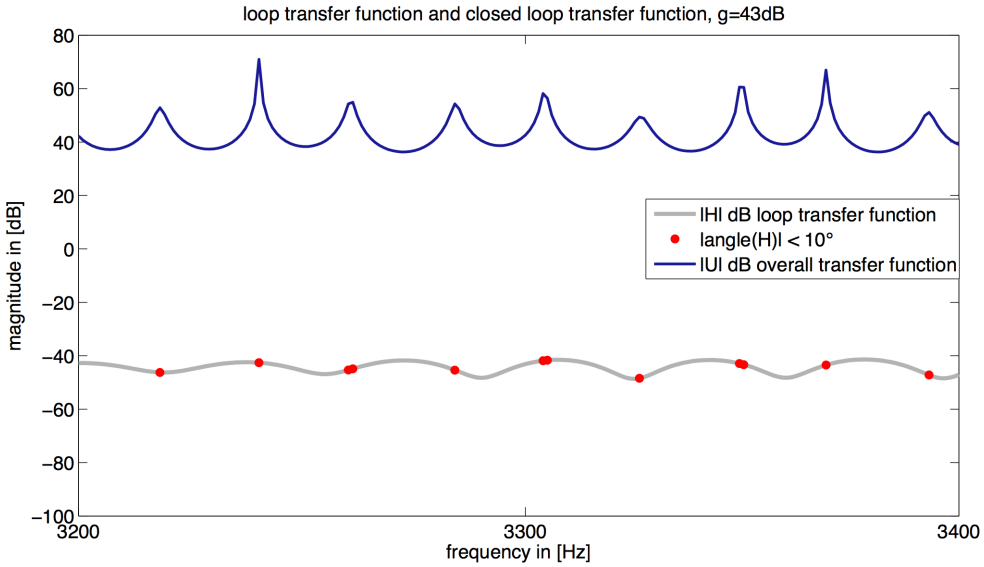

Fig. 3.4: (b) loop and closed loop transfer function in the peak region

[Fig. 3.4 (a)] shows in detail the correlation between low phase shifts and the magnitude

of the closed loop transfer function. From [Fig. 3.4 (b)] can be seen that the zero-crossings of the phase take place in intervalls of less than 100 Hz. Consequently, the magnitude criterion still provides a good estimation of the frequency region in which feedback will occur. Therefore, all MSG calculations in the following examples are based on the magnitude criterion, i.e. the maximum value of the loop transfer function.

Although investigating the closed loop transfer function in the frequency domain cannot contain any information about the pre-assumed stability of the system, it can still be observed that, for gain factors near the maximum stable gain, strong artefacts in the in form of narrow peaks occur. This matches with observation of practical applications, where feedback frequencies are often perceived as notch-effects even in a stable mode of operation. Similar observations have been made in the real time implementation of the simulation in *PureData*. [HL03] have categorized the manifestations of acoustic feedback in hearing aids into three stages, which basically correspond to observations in other acoustic applications:

- Stage 1 - *Stable*: No audible feedback artifacts
- Stage 2 - *Sub-oscillatory feedbacks*: Distortion of the signal, but no steady howling
- Stage 3 - *Self-oscillation*: Steady howling resonances at one or two primary frequencies
- Stage 4 - *Saturation*: Loud, steady howling that provokes the saturation of the device and leads to further distortions

3.3. Analysis of the overall impulse response

As described in *Chapter 2.2*, the inverse Fourier transform of an unstable system does not exist, hence maps to a non-causal impulse response. [Fig. 3.5] and [Fig. 3.6] show

the overall transfer functions and the corresponding inverse Fourier transforms for a gain value below and above the maximum stable gain. As expected, the impulse response of the unstable system shows strong non-causal components and does not seem to decay towards zero.

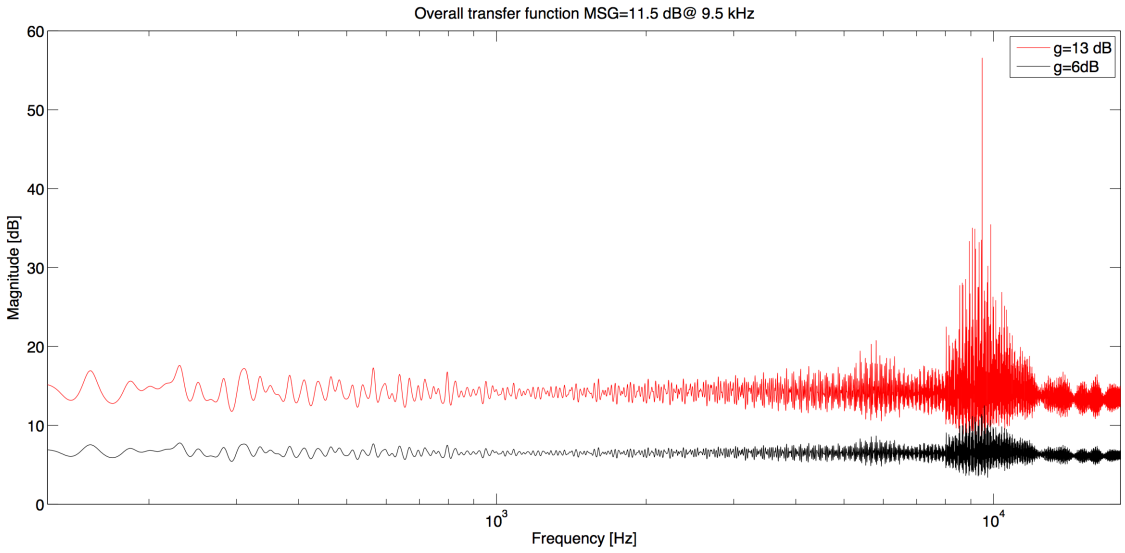

Fig. 3.5: overall transfer function for gain values below and above the MSG

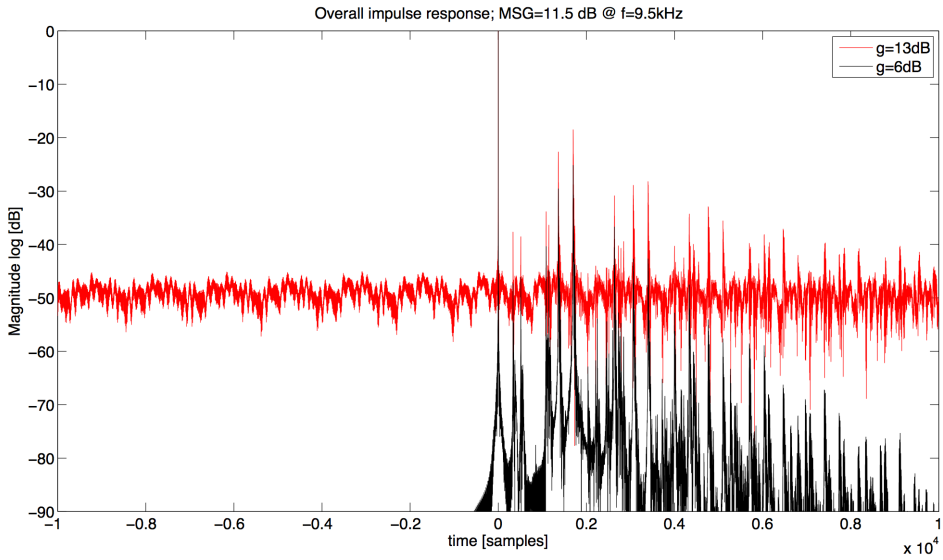

Fig. 3.6: overall impulse response for gain values below and above the MSG

A closer insight into to the behavior of the impulse response can by provided by a frequency-selective analysis of the decay time. From [Fig. 3.7] it can be seen, that the

impulse response in the 800Hz band decays for both gain values towards -100dB, with a slightly increasing decay time for the higher gain value. In the 10kHz band, the curve decays for a value below the MSG but with a longer decay time than in the lower frequency band. When the gain is raised above the stability boundary, the impulse response in this band does not decay further than -20dB in the observed time. This frequency area around 10kHz was also previously detected as the feedback prone region of the system.

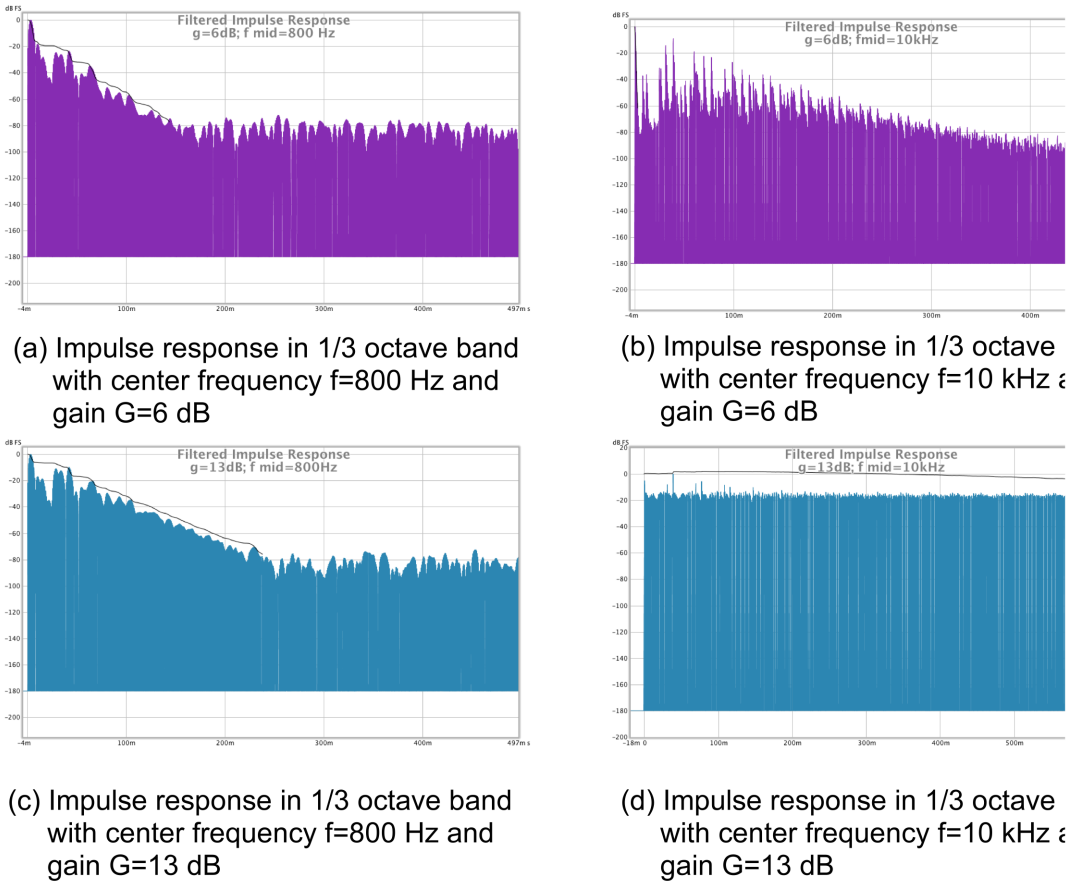

(a) Impulse response in 1/3 octave band with center frequency f=800 Hz and gain G=6 dB

(b) Impulse response in 1/3 octave with center frequency f=10 kHz a gain G=6 dB

(c) Impulse response in 1/3 octave band with center frequency f=800 Hz and gain G=13 dB

(d) Impulse response in 1/3 octave with center frequency f=10 kHz a gain G=13 dB

Fig. 3.7: impulse response decay for different frequency bands and gain values

A different example [Fig. 3.8] shows, that elevations in the loop transfer function result in an increased reverberation time in these distinct frequency bands of the overall impulse response.

These observations correspond to the perception of a „ringing“ in the feedback prone frequency ranges for increasing gain values.

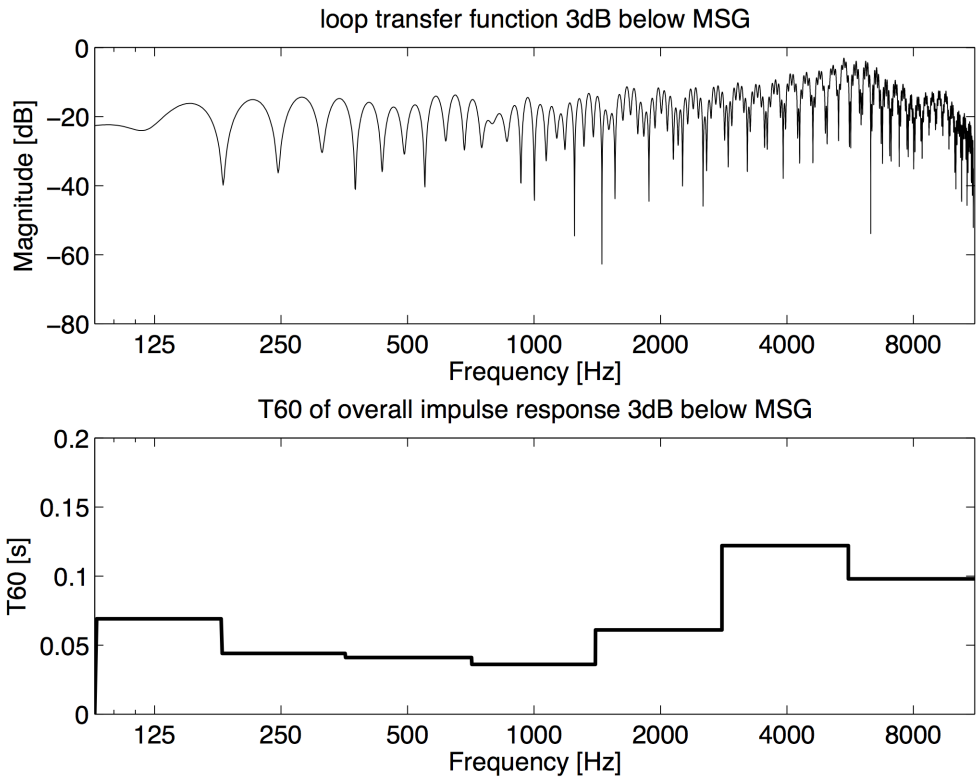

Fig. 3.8: overall impulse response decay and loop transfer function

In a different attempt, a loop transfer function for a room of 45m^3 with a maximum stable gain of 3dB at a frequency of 5.4 kHz was placed in the feedback network and the T60 decay time of the overall impulse response was measured without previous filtering. A convolution with a voice sample, showed, that at a gain of 1dB - 2dB below the feedback limit - resonances could be heard. [Tab. 3.1] shows the corresponding T60 decay times for increasing gain values. For a gain of 3dB, similar to the previous examples, the impulse response did not decay below -60dB within the observed time of 0.5s. The T60 value of 2.4s was obtained from an extrapolation.

Gain	T60
0 dB	0.24 s
1 dB	0.32 s
2 dB	0.65 s
3 dB	2.14 s (*)

Tab. 3.1: Reverberation time for increasing gain values

The decay time of 0.32s, at wich artifacts become noticeable, coincides more or less with the suggested reverberation time of a room used for speech from [FV03]. An extrapolation of the curve leads to a value of 0.3s for a room volume of 45m^3. The gain value, at which the decay time of the overall impulse response reaches the value of suggested reverberation time, can therefore be seen as the MTG, the maximum tolerable gain, at which no artefact can be heard.

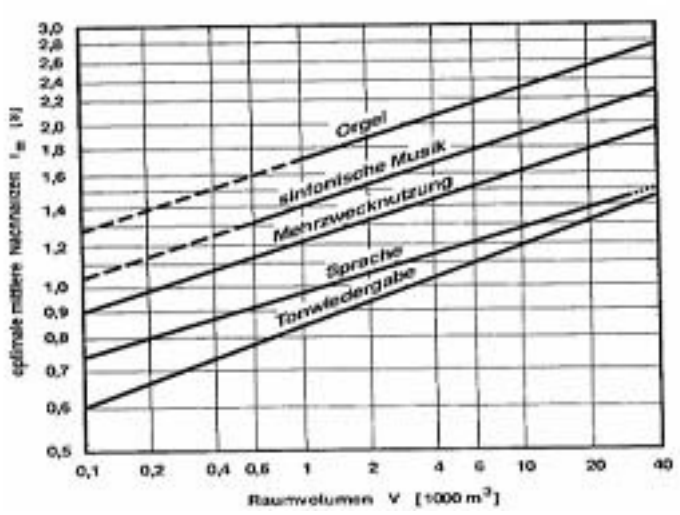

Fig. 3.9: Suggested reverberation times for different room volumes [FV03]

3.4. Equalization of the loop transfer function

Equalization of the input signal, and thereby flattening the loop transfer function, is still the common method to avoid acoustic feedback problems in sound reinforcement systems. The usual process is, to first increase the gain towards instability and then recognize the feedback-prone frequency range - by simply hearing or with the help of a spectral analyzer - and then applying a notch filter. When the gain is increased again, the next ringing will be heard at a higher gain and a different frequency. Which can again be filtered.

By contrast, inspection of a measured loop transfer function has the advantage, that filter parameters can be adapted according to the shape of the peaks. Furthermore, the influence on the overall transfer function can be investigated.

The black curve in [Fig. 3.10] shows a loop transfer function with a calculated MSG of 9.5 dB at a frequency of 4.2 kHz. The highest peak s around 4 kHz eems to be rather broad in the area. Also, two further peaks around 8 kHz can be observed. In a first approach to flatten the transfer function, a notch filter with an attenuation of 9dB and a mid frequency of 4.2 kHz was used. In the resulting blue curve, the highest peak around 4.2 kHz has been eliminated and the MSG has been increased to 13.7 dB. By using a second notch filter with a mid frequency of 8.5 kHz, the loop transfer function can be further flattened, and an increase in the maximum stable gain to 16.7 dB can be accomplished. By eliminating the two main peaks with simple notch filters, more than 7 dB headroom has been gained. Of course, the complexity of the necessary filtering strongly depends on the shape of the loop transfer functions.

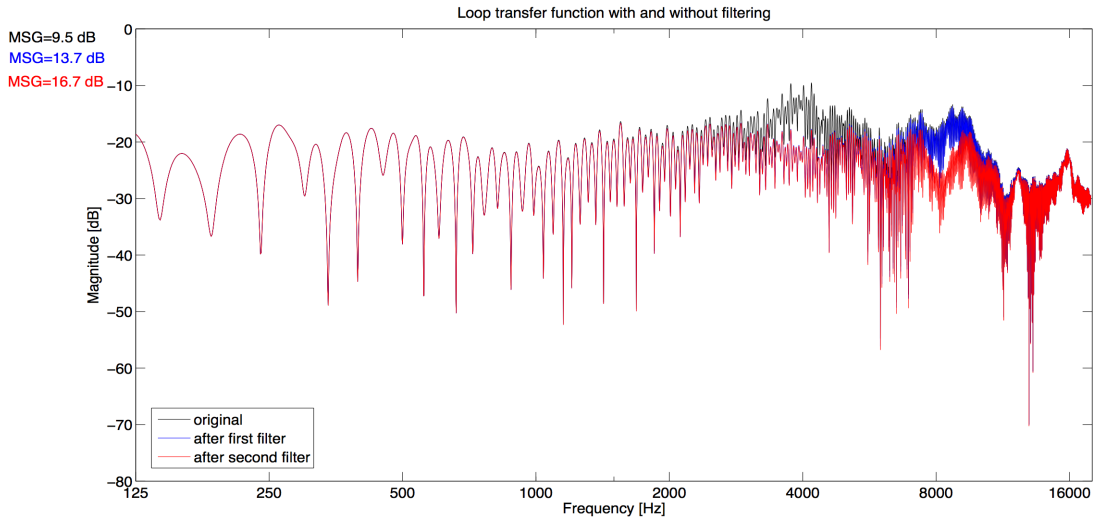

Fig. 3.10: Loop transfer function with and without filtering

Let us take a look at the effects on the overall transfer function of a feedback network with a gain of 15 dB. Since, from a practical point of view, the filter F has to be inserted into the main path, the resulting overall transfer function can be calculated as:

(3.1)
$$H_{filtered} = \frac{g \cdot F}{(1 - F \cdot L \cdot g)} \quad .$$

Although the frequency response of the overall system does not give detailed information about the stability of the system, it can thus be seen from [Fig. 3.11] that

strong howling resonances near the peaks of the loop transfer function disappear in the overall transfer function when the loop is flattened.

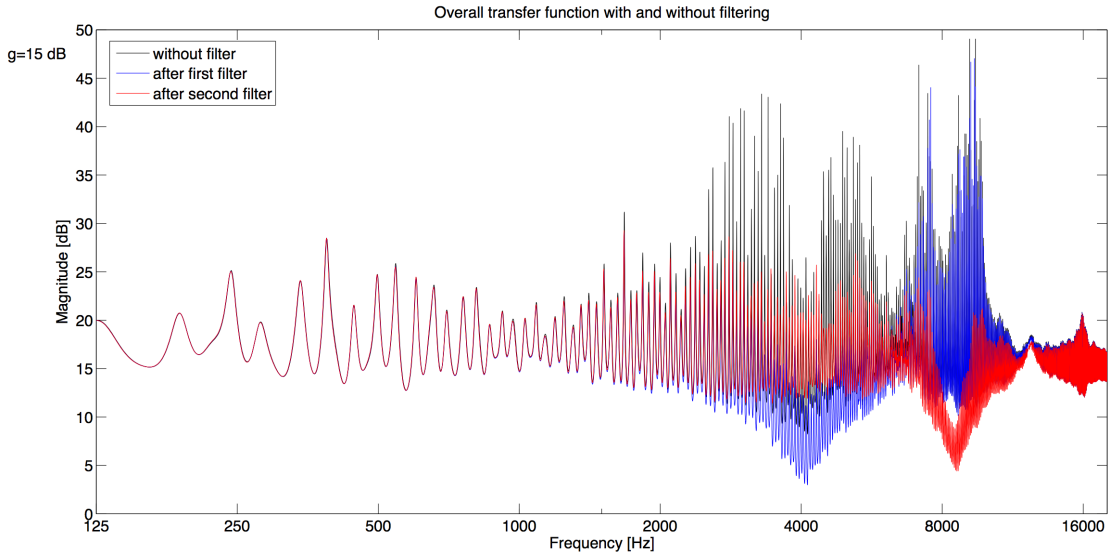

Fig. 3.11: Overall transfer function with and without filtering

When using filters in feedback networks, the influence of the phase response of the filter is an important issue: As shown before, the occurrence and strength of a resonance strongly depends on the phase of the loop transfer function. If a filter has strong variations in phase, the exact locations of the howling resonances in the overall transfer function can change.

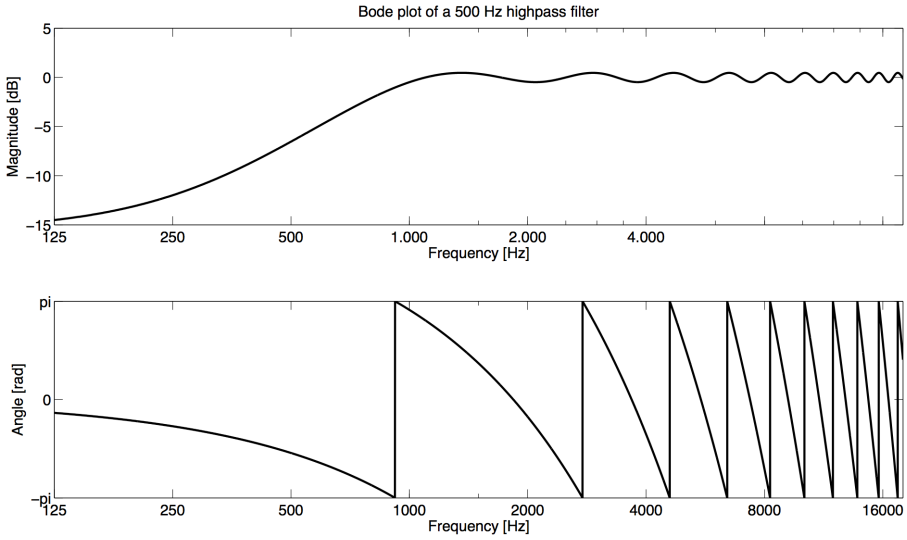

Fig. 3.12: Bode plot of a high-pass filter

The above applied notch filters have a zero phase response except closely around their center frequency. Therefore the resulting influences on the overall feedback network are rather small. For example a high-pass filter has a varying, phase response, which can be seen in the bode plot [Fig. 3.12].

When this filter is placed in the overall feedback network, the phase of the loop transfer function changes and therefore the locations of the audible resonances. The effect of such a phase response is illustrated in [Fig. 3.13].

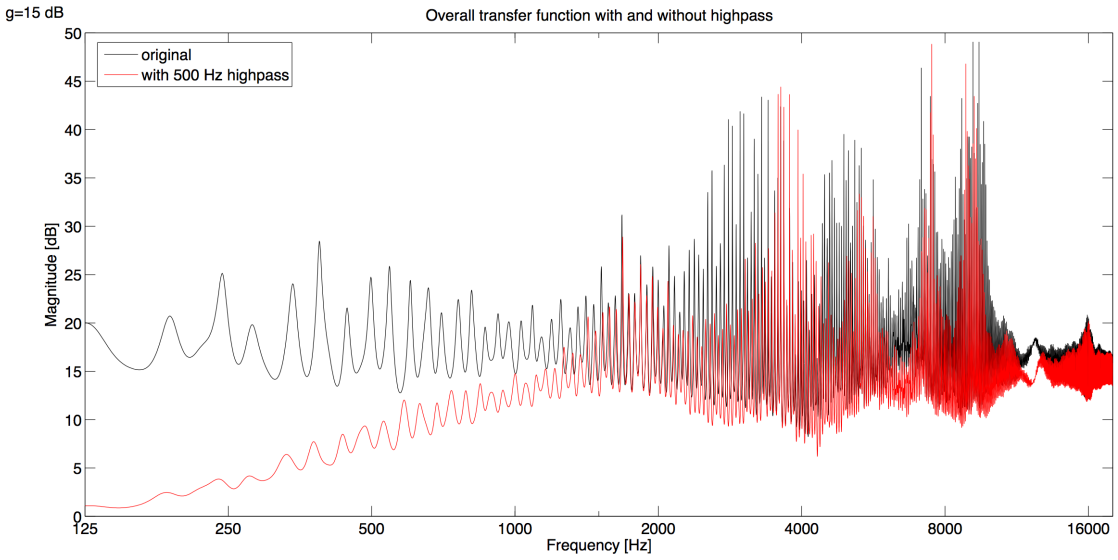

Fig. 3.13: overall transfer function with and without high-pass filter

Resulting from this observation the conclusion can be drawn that filters with a non-zero phase response modify the feedback behavior, even if the magnitude remains unmodified. Of course this is also the case for other signal processing devices in the signal chain which affect the phase response.

While the magnitude criterion provides a good estimation of the frequency range at which resonances occur, the exact feedback frequency can only be detected in combination with the phase criterion.

3.5. Rehearsal room monitoring situation

A standard monitoring situation shall now serve as a first example for the following parameter and simulation variations. A dynamic super-cardioid microphone (*AKG* D7) and stage monitor (*JBL SRX 712M*) are placed in a room of the dimensions 6m x 5m x 3m according to [Fig. 3.14], where the microphone is located at a hight of 1.8m and the loudspeaker at 2m. All walls have a low average absorption coefficient – the frequency dependent values for wallpaper [Appendix A] were used. The setup represents a reverberant rehearsal room.

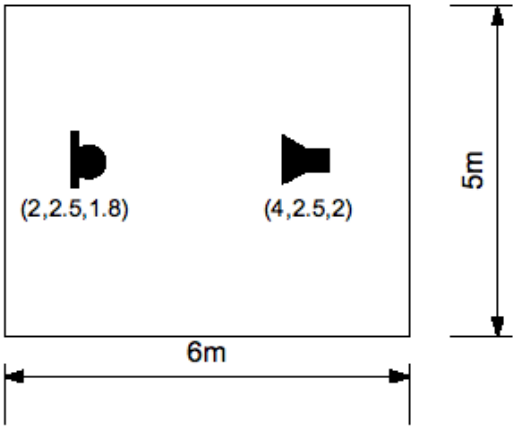

Fig. 3.14: Schematic illustration of the monitoring setup

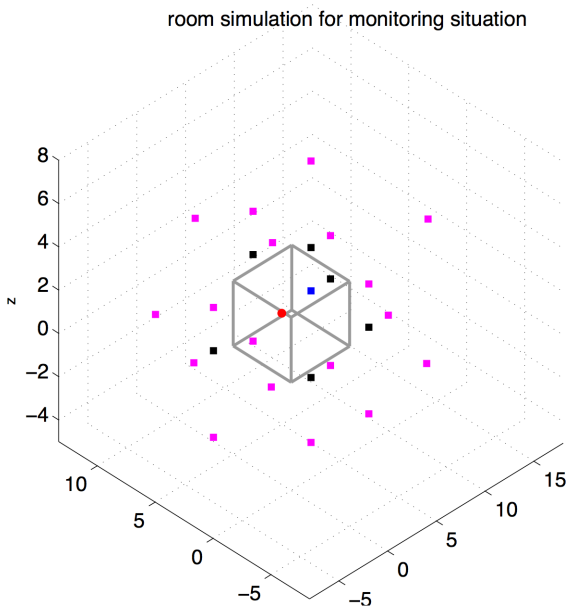

Fig. 3.15: Simulated room with first and second order mirror sources

[Fig. 3.16] shows the simulated room transfer function. The maximum stable gain for this example was calculated to be 13.33 dB with a peak frequency at 5.64 kHz.

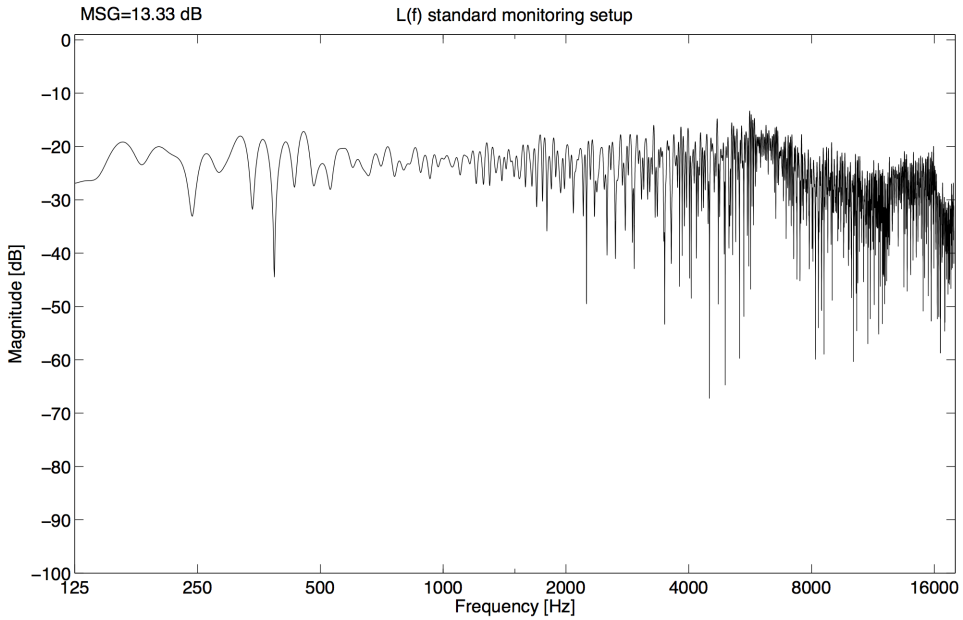

Fig. 3.16: Loop transfer function for rehearsal room monitoring example

3.6. Importance of determining factors in the simulation

Phase information and time delay

As described in *Chapter 2*, in previous work the importance of using the complex frequency response of microphone and loudspeaker, i.e. including the phase information, has been pointed out as important. To investigate the impact of the phase data regarding this simulation method, the monitoring setup as described above has been implemented twice, once considering the phase responses and another time neglecting them. In a third approach, also the linear phase time delay due to direct and mirror sources was omitted. [Fig. 3.17] shows the loop transfer functions of all three implementations.

When only the absolute value of transfer functions of the directional sources and the

microphone are used (red curve), the shape of the loop transfer function L(f) slightly changes: Constructive and destructive interferences still take place due to the delay of the arriving sound of the mirror sources, but at different frequencies. Still, the calculated MSG remains in the same range as for the previous calculation where the phase is considered. Also at other frequencies, the error made is relatively small, considering the tendencies of the overall frequency response curve.

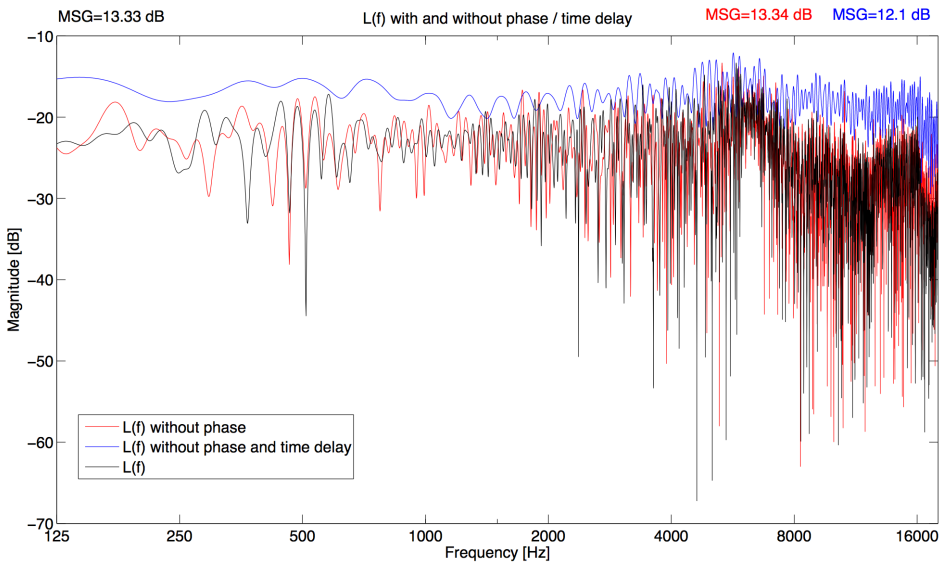

Fig. 3.17: L(f) function when phase and time delay are considered / omitted

When the time delay of the arriving sound is also neglected (blue curve), all interferences are constructive. The result is a smoother shape of the loop transfer function and a lower calculated MSG value, in this example 12.1 dB without phase and time delay vs. 13.33 dB from the previous calculation. The error is especially significant in the low frequency area, where the magnitudes show a difference of up to 15 dB.

The small difference for the first and experiment indicates, that even with the absolute values of the directivity patterns, a good estimation of the loop transfer function can be obtained. The consideration of the time delays of arrival for the different sources on the other hand is necessary to gain sensible results for the MSG value and the estimation of howling tendencies.

Image source order

Up to this point, both first and second order image sources were taken into consideration when simulating the room impulse response. It is obvious that the room model becomes more accurate when the image source order is increased, but the question arrises, in how far later reflections contribute to the onset of acoustic feedbacks regarding their strong attenuation and also the extended time delay. [TR09] assumes the upper border of the *Haas time* as an intervall of reflections which contribute to the onset of acoustic feedbacks. With c=343m/s this corresponds to a sound path of 10m. In a three-dimensional room with the dimensions 5m x 8m x 3m and the loudspeaker positioned at the coordinates (1,2,2), already one of the first order mirror sources is out of this range. However regarding the levels of the arriving reflections, the mirroring of the directivity patterns have to be taken into account: For sources with a high directivity factor it is likely that second reflections of sound radiated from the main axis are still stronger after their second reflection, than the first one, when the orientation of the main direction of radiation flips.

In this work, a comparison between first and second order image sources has been carried out with a three-dimensional simulation, to get first impressions about the changes taking place when increasing the order. [Fig. 3.18] shows a comparison of the loop transfer function for the monitoring example introduced in *Chapter 3.3* simulated with first and second order image sources.

Second order image sources generally contribute to a higher magnitude level and a stronger degree of interference determining the fine structure of the frequency response. As a consequence, the maximum stable gain for first order image sources is calculated at about 3.7dB higher. For low frequencies, the difference in magnitude amounts to about 7dB. Despite a higher image source order improves the accuracy of the calculation, a larger attenuation of higher order image sources can be expected due to absorption and distance.

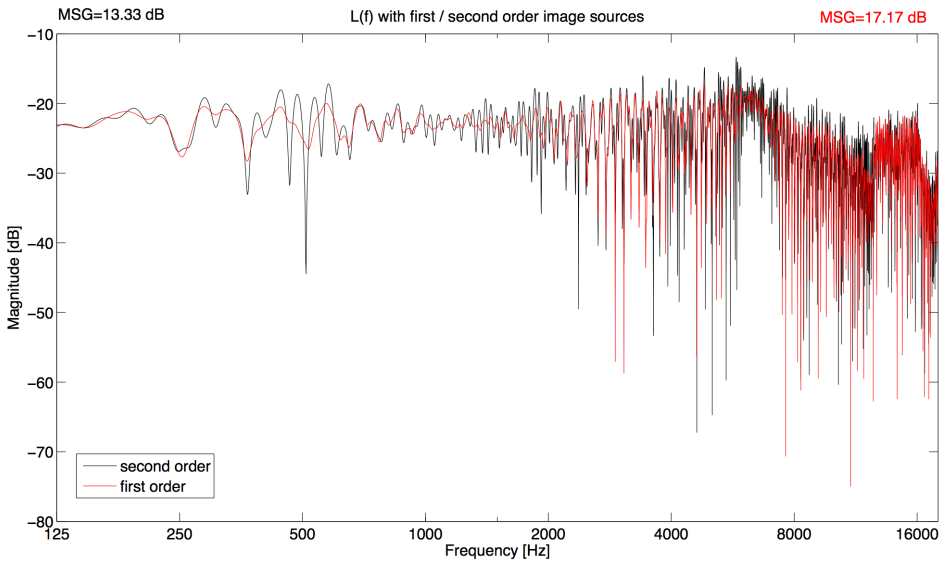

Fig. 3.18: L(f) function for first and second order image sources

Diffuse field

In the example of the monitoring scenario in a rather reverberant environment, it is interesting to investigate the importance of the modeling of the diffuse field. Therefore, [Fig. 3.19] shows the loop transfer function of a simulation approach without the presence of the diffuse field. In this example, the absence of the diffuse field results in a lower magnitude and the maximum stable gain was calculated to lie at about 3.8 dB higher.

For low frequencies, both microphone and loudspeaker show a more omnidirectional behavior. Hence, the influence of the diffuse field on the loop transfer function is especially strong in the low frequency range, resulting in an error of up to 20 dB when neglecting the diffuse field. Additionally, due to the relatively reverberant environment, the diffuse field response has a strong influence on the envelope of the loop transfer function and contributes strongly to the peak detection.

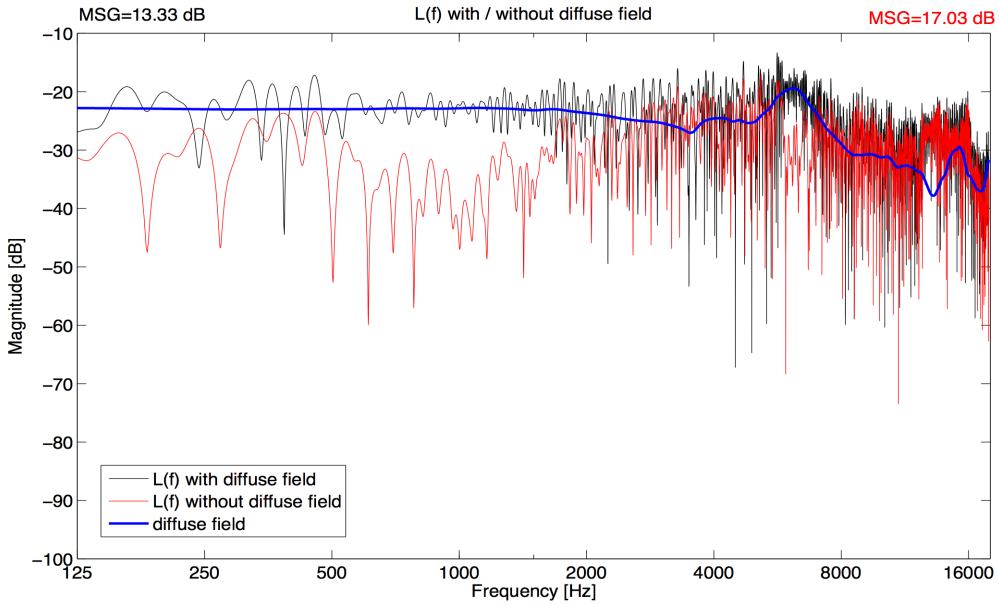

Fig.3.19: L(f) with and without diffuse field

3.7. Influence of absorption and room parameters

Room volume

To find out more about the relation between the room volume and the feedback behavior, the maximum stable gain for different room sizes has been determined using the standard monitoring scenario described in *Chapter 3.5* [Fig. 3.20] shows the results. Microphone and loudspeaker were placed in the center of the room width, keeping their distance between them and the distance between microphone and the adjacent wall constant.

A larger room surface results in a greater critical distance hence a lower diffuse field. Furthermore, the distance from the microphone to several image sources increases so that the reflected sound arrives at a lower level. It is therefore assumed that the maximum stable gain increases by increasing room size. When the room size tends towards infinity, the behavior of the loop transfer function corresponds to free field

conditions, meaning that the maximum stable gain is solely determined by the direct path between microphone and loudspeaker.

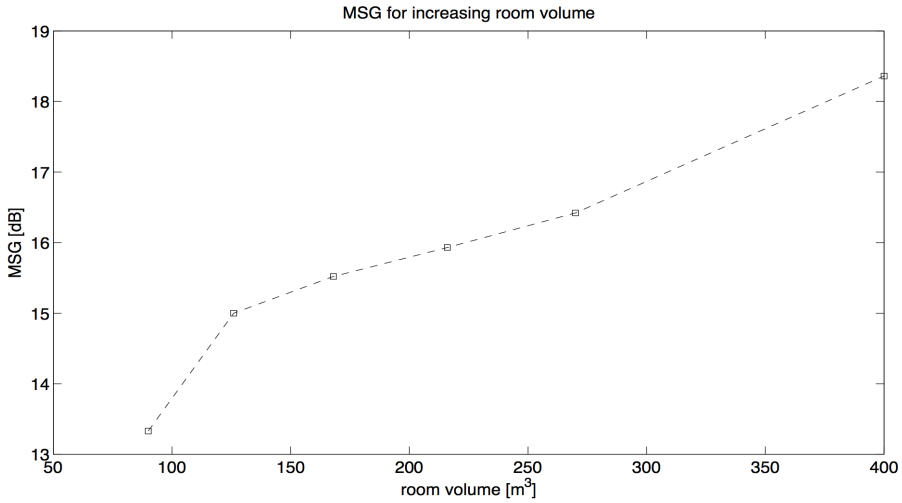

Fig. 3.20: MSG for different room sizes

The simulation results [Fig. 3.20] show a general tendency towards this behavior, but the relation is not strictly proportional. When the room size is increased, also the positions of the image sources and consequently the angles from and to the microphone change. As a result, the angle-dependent microphone and loudspeaker frequency responses can cause an alteration of the loop transfer function.

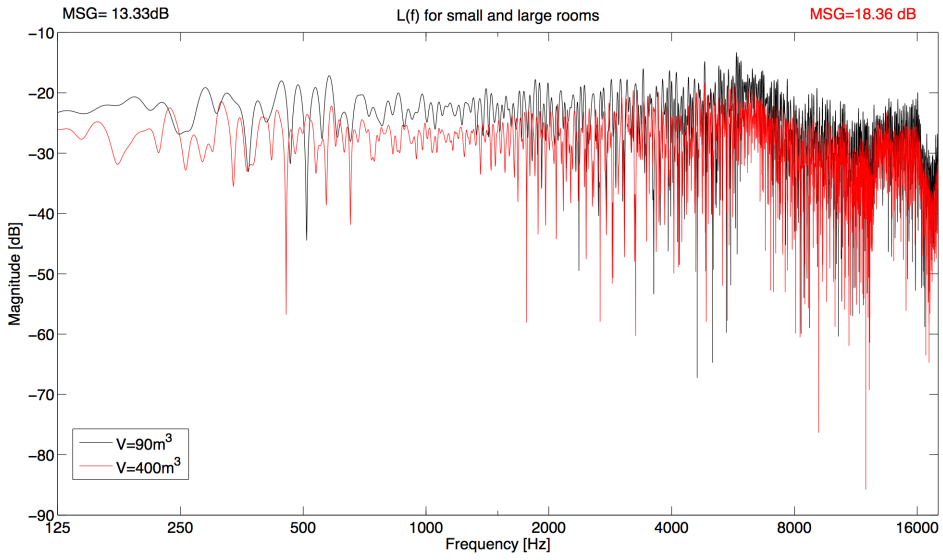

Fig. 3.21:Loop transfer function for two different room sizes

[Fig. 3.21] shows, as an example, the loop transfer function of an increased room volume compared to the standard monitoring setup. The relatively small changes in the fine structure of the frequency response cause the non-linear behavior of the relation between maximum stable gain and room size

Room shape

Especially for room acoustic consulting, it is interesting to find out in how far the shape of a room influences the feedback behavior. Therefore, the room shape of the monitoring situation has been modified according to [Fig. 3.22], while keeping the room volume contant.

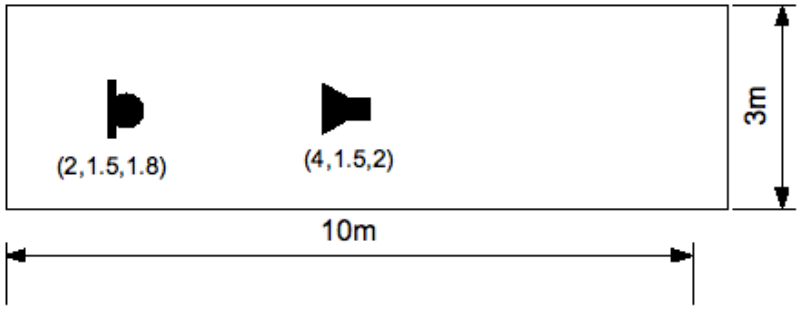

Fig. 3.22: Modified room shape for monitoring scenario

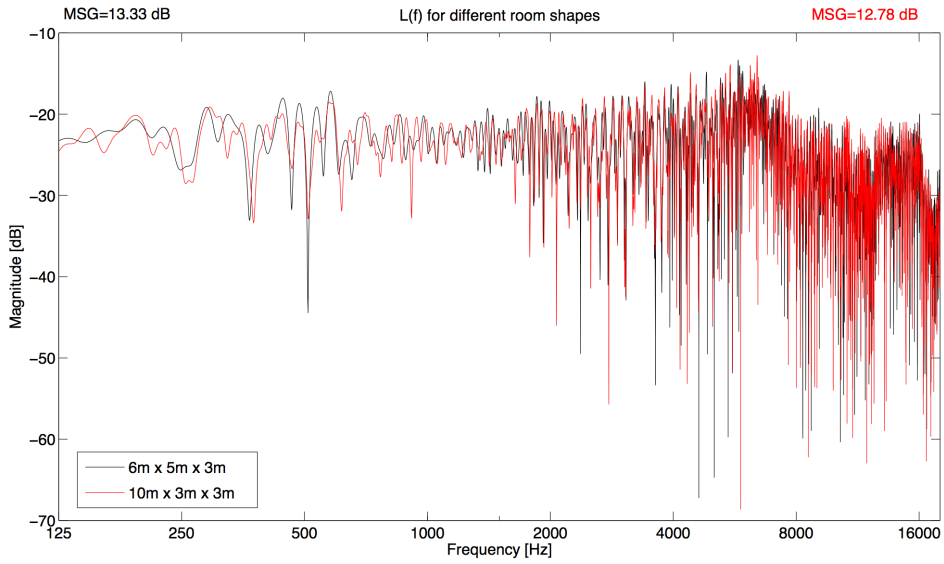

Fig. 3.23: L(f) for original (black) and modified (red) room shape

[Fig.3.23] shows the loop transfer function of the modified room compared to the original setup. The changes are rather small in the entire frequency range and the maximum stable gain has increased by less than 1 dB.

Especially in the low frequency area, the modification of the room shape causes changes of the room modes, which are excluded from the present simulation model.

The frequencies at which the n^{th} order modes occur depend on the room dimensions width w, length l, and hight h and can be calculated from the sonic speed c as follows:

$$f = \frac{c}{2} \cdot \sqrt{\left(\frac{n_l}{l}\right)^2 + \left(\frac{n_w}{w}\right)^2 + \left(\frac{n_h}{h}\right)^2} \quad . \tag{3.2}$$

Absorption

To investigate the influence of wall absorption materials on the feedback behavior, two extreme variations of the monitoring scenario have been implemented: The standard monitoring situation with rigid walls and the same setup with strongly absorbing acoustic panels.

Here again, a previous assumption can be made that highly absorbing materials on the wall surfaces cause a higher maximum stable gain because the mirror sources lose are attenuated.

As [Fig. 3.24] shows, the increase of the absorption yields an improvement of the maximum stable gain of about 3 dB in the given example. [Tab. 3.2] shows the calculated maximum stable gain values for various wall materials. Significant improvements between 2 and 3.5 dB can only be observed when walls are equipped with strongly absorbing materials.

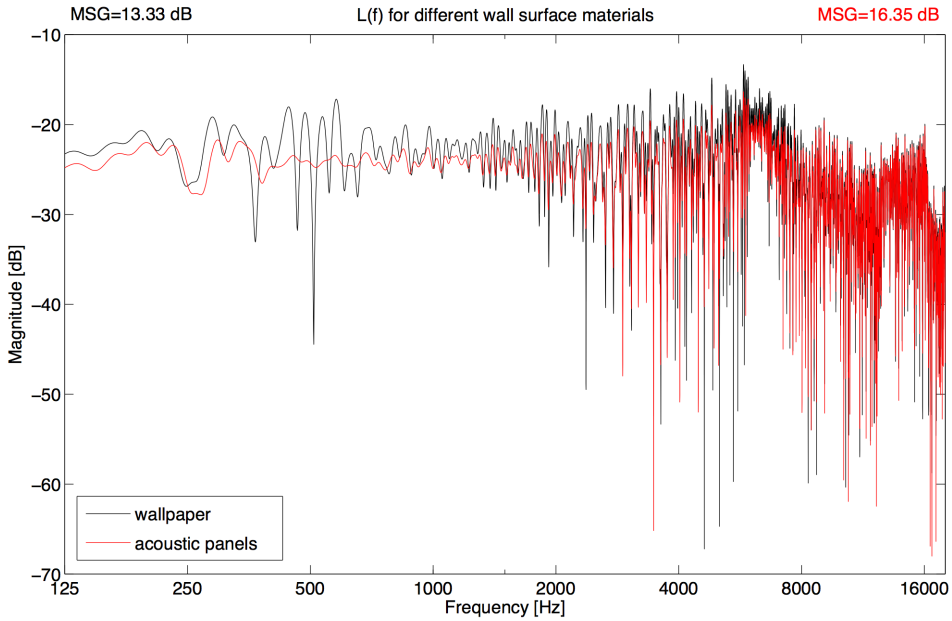

Fig. 3.24: Loop transfer function for different wall surface materials

Material	MSG
Brick wall	13.62 dB
Wood	13.32 dB
Wallpaper	13.33 dB
Curtain	16.87 dB
Glass	13.30 dB
Helmholtz absorber	15.16 dB
Acoustic panel	16.35 dB

Tab. 3.2: MSG for two different wall surface materials

For practical applications, it is not efficient to modify all surface materials just to improve the feedback behavior, especially regarding costs and visuals aspects. A treatment of the most important wall reflections that might cause feedback, i.e. the upper back wall and ceiling part of a stage, in combination with suitable directivity patterns can efficiently avoid feedback.

Moreover, the frequency dependence of the absorption coefficient is of great importance. Helmholtz absorbers for example have the effect of a notch filter, i.e. other

frequency ranges are affected less and useful components of the early reflections are not being destroyed. From a practical aspect, it is still virtually impossible to equip an entire room with this kind of material. But, for fixed installations, a so-called spot treatment is thinkable, where absorbing material is positioned at the crucial points of reflection.

3.8. Robustness of the loop transfer function

In literature, for example [WM09], it is stated, that the room transfer function undergoes heavy modifications when small changes to the source or receiver position are applied. Therefore, some simulations have been carried out to find out more about the robustness of the loop transfer function due to small positional and rotational changes. In particular this is done to investigate in how far the calculated MSG and the peak frequency are affected.

Rotational changes of the microphone orientation

In a first example, the orientation of the microphone has been slightly changed in steps of 5 degrees from 150° to 180°. [Tab. 3.3] shows the calculated maximum stable gain and the peak frequencies for all simulated microphone angles.

For these small rotational changes, the maximum stable gain varies less than 1.5 dB and the peak frequency remains in a range of 100 Hz, corresponding to the tendency of the peak of the envelope in the loop transfer function of the monitoring example. It was mentioned before that by flattening the loop transfer function, the MSG of the overall system can be improved. Since the envelope of the loop transfer function is robust to changes of the rotation, improvements can be obtained with a static filter, even if the microphone is rotated during the performance.

If the orientation of the microphone is strongly changed to 0°, the direct sound of the source arrives on-axis, where the microphone exhibits the largest sensitivity. For this

case, a MSG of 0.8 dB is calculated. This corresponds to the common observation, that the *Larsen* effect suddenly becomes audible when, e.g., a speaker points the microphone towards the loudspeaker. [Fig. 3.25] shows the overall transfer function of this scenario for a gain factor of 6 dB.

Microphone rotation [deg]	MSG [dB]	Peak frequency [Hz]
180	13.33	5643
175	13.21	5643
170	13.32	5691
165	13.03	5691
160	12.74	5691
155	12.43	5742
150	11.97	5742

Tab. 3.3: MSG for different microphone rotation angles

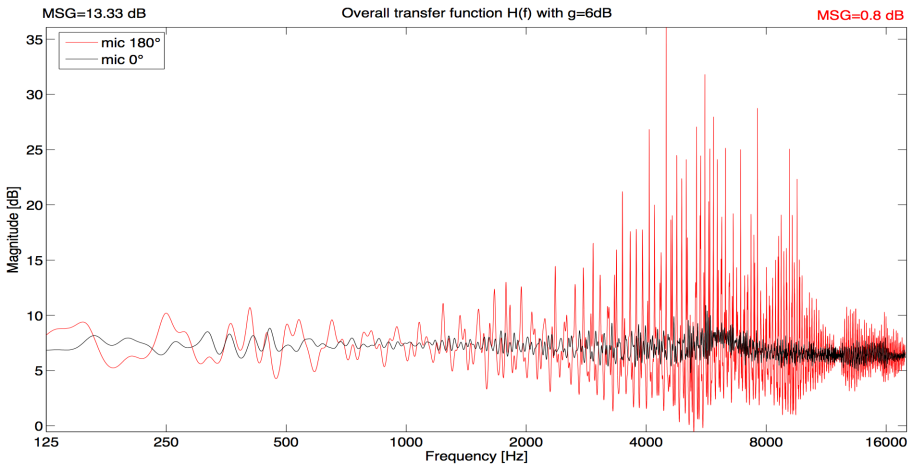

Fig. 3.25: Overall transfer function for different microphone rotations

Rotational changes of the loudspeaker orientation

Especially for fixed installations, it would be interesting to know in how far an improvement of the feedback behavior can be obtained by choosing a specific

loudspeaker angle. [Tab. 3.4] shows the calculated maximum stable gain for loudspeaker angles between 150 and 180 degrees.

The results show a similar relation as for the microphone rotation. Hence, the loop transfer function seems to be relatively robust to rotational changes. The advantage is, that equalization will show good results, even if changes in the orientation take place. On the other hand, a modification of the orientation will not lead to a significant improvement of the feedback behavior in fixed installations.

Loudspeaker rotation [deg]	MSG [dB]	Peak frequency [Hz]
180	13.33	5643
175	13.12	5644
170	12.56	5690
165	12.39	5690
160	12.66	5690
155	12.51	5691
150	11.78	5692

Tab.3.4: MSG and peak frequencies for different loudspeaker rotations

Positional changes

In sound reinforcement systems it is very likely that the microphone is being moved during a performance. It is therefore interesting to investigate the influence of positional changes on the loop transfer function and the MSG.

In a first approach, the microphone was moved further away from the loudspeaker. [Tab. 3.5] shows the maximum stable gain for different spacings of microphone and loudspeaker. It becomes obvious, that there is no linear relation between the distance and the maximum stable gain. Only for close spacings of less than 2.4m, the MSG actually increases with the distance. In this range, the loop transfer function is

dominated by with 1/d decreasing field of the direct source. With an increasing distance, the influence of the diffuse field and the mirror sources becomes proportionally greater. Especially the reflection at the wall behind the microphone is relatively strong since it comes from the main axis of the speaker. Consequently, the attenuated direct sound is partly compensated by the higher level of reflected sound. Furthermore, larger differences can be observed in the detected peak frequencies. The peak frequency of the loop transfer function varies in a range of about 1.6 kHz.

Distance [m]	**MSG [dB]**	**Peak frequency [Hz]**
1	12.02	5380
2	13.33	5643
2.2	13.92	6068
2.4	12.65	6253
2.6	13.7	6008
2.8	11.94	5514
3	12.75	5289
3.5	12.64	4594

Tab. 3.5: Maximum stable gain for an increasing distance between microphone and loudspeaker

The procedure is now being repeated for a displacement of the microphone on the y and the z axis from the initial situation of both microphone and loudspeaker being on the y-position and height.

[Tab. 3.6] shows the values of the MSG for the different microphone positions. The results show, that changes take place within a range of 2 dB. Again, the slightly increasing distance to the loudspeaker seems to be partly compensated by the higher influence of the image sources at the side walls or the floor reflection when the hight of the microphone is lowered. Although the envelope of the loop transfer function remains basically unaffected, the peak frequency varies within the range of the rather broad main peak, namely between 4.5 kHz and 6.2 kHz. This range though, could still be covered using a broader notch filter.

Again, the room modes are not included in this simulation, but cause strong modifications of the loop transfer functions in case of a displacement of the microphone. If the microphone is e.g. moved from an antinode to a node of a standing wave, the level of this particular frequency will suddenly increase.

Δy	**MSG [dB]**	**f_{Peak} [Hz]**	**Δz**	MSG **[dB]**	**f_{Peak} [Hz]**
0	13.33	5643	0	13.33	5643
0.2	15.03	4785	0.2	12.99	5731
0.4	14.15	6147	0.4	14.82	5765
0.6	14.64	5774	0.6	14.96	6036
0.8	14.67	4897	0.8	13.40	6110
1	14.69	6079	1	14.57	5512
2	14.69	6079	1.5	14.06	5691

Tab. 3.6: MSG and peak frequencies for positional modifications

The distance **Δ**x between node and antinode can be calculated for an arbitrary frequency f with the speed of sound c:

(3.3) $$\Delta x = \frac{\lambda}{4} = \frac{f}{4 \cdot c} \quad .$$

Consequently, for a room mode at a frequency of 100 Hz, a positional change of 72 cm is sufficient to move the microphone from a node to an antinode.

3.9. Influence of microphone and loudspeaker characteristics

Frequency characteristics

This chapter deals with the question in how far microphone and loudspeaker frequency characteristics have a general influence on the occurrence of acoustic feedbacks. Similar

to the idealized setup in *Chapter 3.1*, we will therefore take a look the theoretical scenario, where microphone and loudspeaker have flat frequency responses to see how the irregularities of microphone and loudspeaker frequency characteristics contribute to the maximum stable gain. In this example as distinct from *Chapter 3.1*, the microphone and the loudspeaker are not assumed to be omnidirectional. To model an angle dependent magnitude attenuation, the attenuation at a frequency of 1kHz has been used and the phase was set to zero:

(3.4) $$\left|M(\varphi, f)\right| = \left|M(\varphi, f = 1\text{kHz})\right| \quad ,$$

(3.5) $$arg\left(M(\varphi)\right) = 0 \quad ,$$

(3.6) $$\left|S(\varphi, f)\right| = \left|S(\varphi, f = 1\text{kHz})\right| \quad ,$$

(3.7) $$arg\left(S(\varphi)\right) = 0 \quad .$$

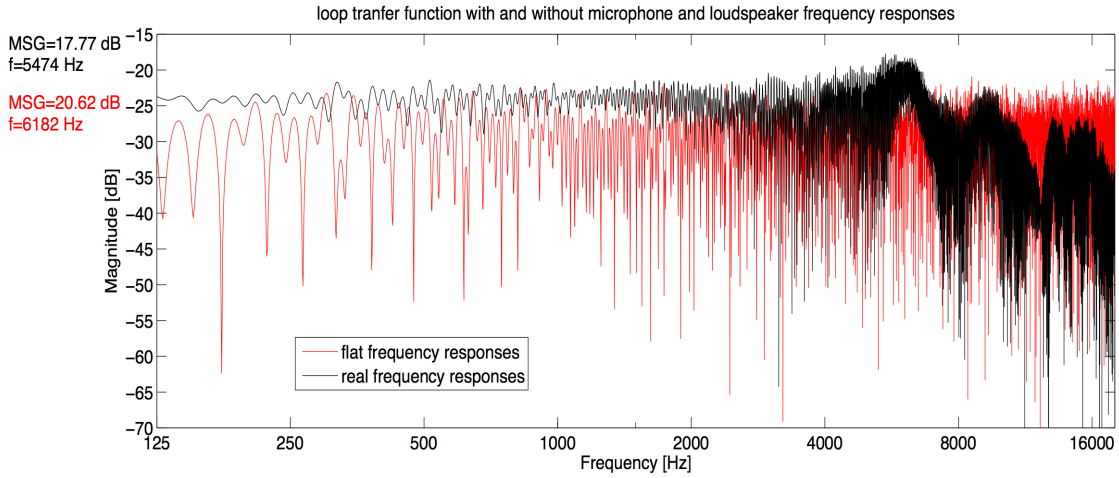

Fig.3.26: Loop transfer function for flat and real frequency responses

[Fig. 3.26] shows the loop transfer function for flat and real frequency responses. When neglecting the frequency characteristics of microphone, an increase in the MSG of nearly 4 dB can be observed. The frequency characteristics seem to determine the tendencies of the loop transfer function to a great amount and cause the elevations at which feedback occurs. Consequently, as in audio applications in general, a flat

frequency response of both microphone and loudspeaker is desirable to minimize feedback sensitivity. Or, alternatively, a combination of characteristics, which compensate each other, could be thinkable.

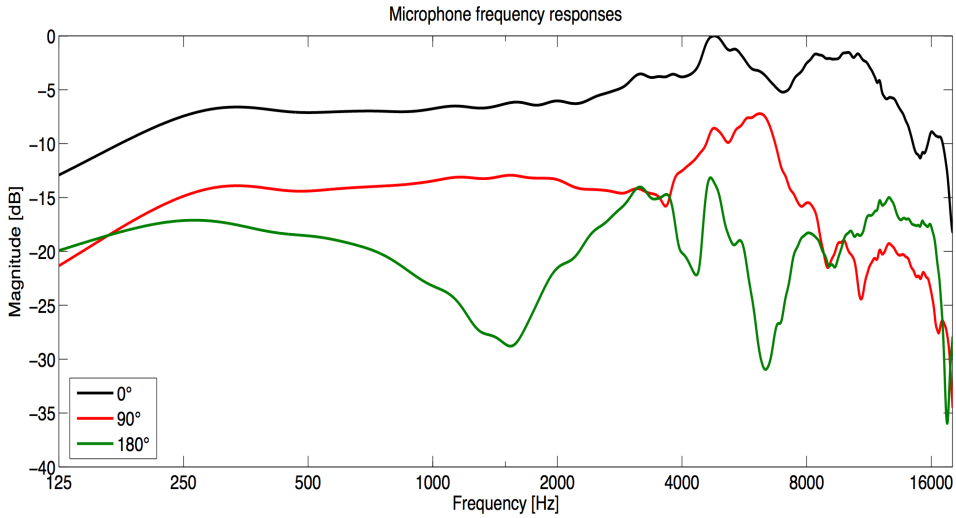

Fig. 3.27: Microphone (AKG D7) frequency responses for different angles

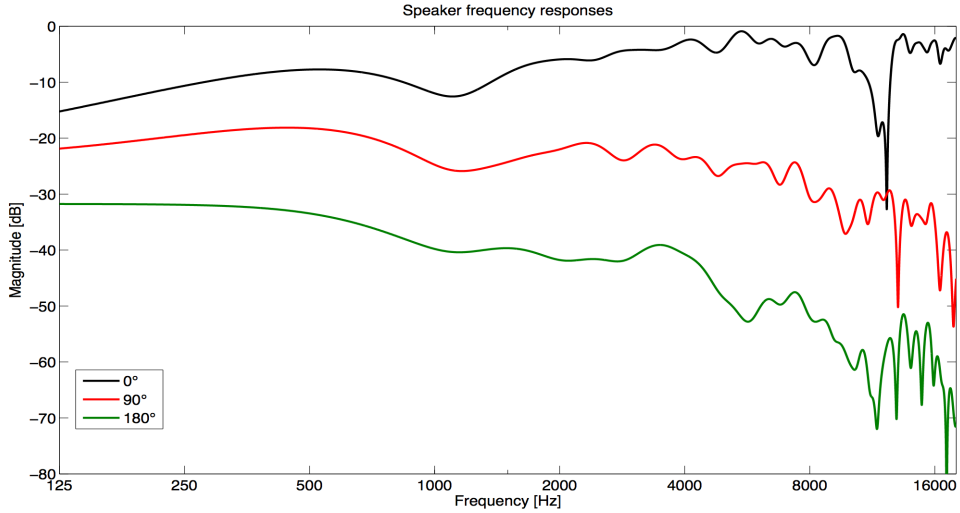

Fig. 3.28: Loudspeaker frequency responses for different angles

[Fig.3.27] and [Fig.3.28] show the frequency responses of the used microphone and the loudspeaker for different angles. It can be seen, that in the range of the peak around 5.5 kHz which occurred in all examples, both microphone and loudspeaker show an

elevation.

Directivity characteristics

It is quite evident, that directional microphones since sound coming from angles other then the main axis is being rejected will in general lead to better results regarding the maximum stable gain than omnidirectional microphones. It is also obvious that, as explained in [Sch71], the choice of microphone depends also on the sound field it is exposed to: A super-cardioid is e.g. not a good choice for a monitoring situation where the monitor is mounted on the same hight as the microphone in a way that the monitor points towards the strong rear lobe of the microphone. [Sch71] also predicted, that with second order cardioids – because of their higher directivity- an increase of 4dB in MSG could be obtained, compared to a regular cardioid microphone. This prediction though, was based on the assumption of a fully diffuse field with the sound energy being equally distributed.

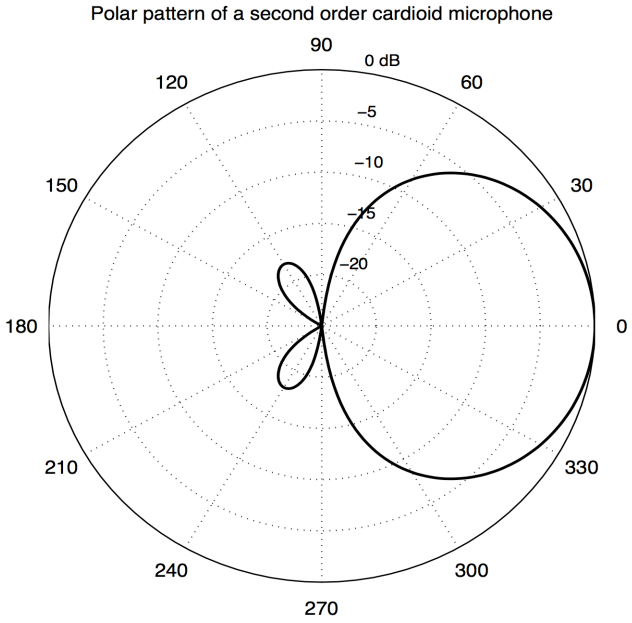

Fig. 3.29: Polar pattern of a second order cardioid microphone

In a simulation approach, the difference between an omnidirectional, a regular and a second-order cardioid microphone [Fig. 3.29] shall be investigated, when both

microphones are assumed to have a stable directivity pattern for the entire frequency range and a flat frequency response.

The angle dependent magnitude can be calculated for the regular cardioid as [Sch71]:

(3.8) $$|M(\varphi)| = 1/2 * (1 + \cos(\varphi)) \quad .$$

The magnitude of the second-order cardioid is given by [Sch71]:

(3.9) $$|M(\varphi)| = 1/2 * (1 + \cos(\varphi)) * \cos(\varphi) \quad .$$

For a monitoring situation, the results [Tab. 3.7] showed small cahnges of the MSG for the second order cardioid. Compared to the omnidirectional microphone, an increase of more than 10 dB can be observed due to the rejection of the reflections arriving from angles other than the on-axis.

MSG		
omnidirectional	**cardioid**	**2nd order cardioid**
2.15 dB	12.84 dB	13.26 dB

Tab. 3.7: MSG for different microphone types

Consequently, the idea was confirmed, that microphones with a high directivity are most qualified for the usage in feedback-prone environments. For practical applications, a compromise has to be found, since highly directional microphones often have rippled frequency responses, which result in peaks in the loop transfer function and can have a negative influence on the sound quality.

3.10. Microphone comparison

Especially from a practical perspective, the question arrises if certain microphones are

more feedback-prone than others. Therefore, measurement data of seven different microphones has been used to compare their performance in feedback-prone environments. [Tab. 3.8] gives a brief overview of their features. The on-axis frequency responses and the polar patterns can be found in Appendix B. To obtain a useful comparison, all microphone frequency responses were normalized in a way, that the on-axis magnitude at a frequency of 1 kHz corresponds to 0 dB.

Furthermore, two stage monitoring scenarios were chosen to compare the the feedback behavior. The plane towards the audience area was let open and it is assumed, that due to the high absorption and the great distance to the next wall, no reflections arrive from the audience area. For the first example, a low reverberation was assumed and therefore the remaining walls we equipped with a highly absorbing material (curtain). In the second example, the distance between loudspeaker and microphone is increased and wood was chosen as a wall surface material, to obtain a more reverberant environment. [Fig.3.30] and [Fig. 3.31] illustrate both stage monitoring setups.

Microphone	**directivity**	**dynamic / condenser**
AKG D7	super-cardioid	dynamic
AKG P5	super-cardioid	dynamic
Shure KSM9	cardioid	dynamic
Neumann KMS105	super-cardioid	condenser
AG C480	cardioid	condenser
AKG CK98	directional	condenser
Shure SM58	cardioid	dynamic

Fig. 3.8: overview of the microphone types used in the comparison

The resulting maximum stable gain for the different microphones can be found in [Tab. 3.9] for example 1 and [Tab 3.10] for example 2, ranked from the best to the worst result. The MSG differs varies in a range 4.2 dB for the first and 5.2 dB for the second example for the various microphone types.

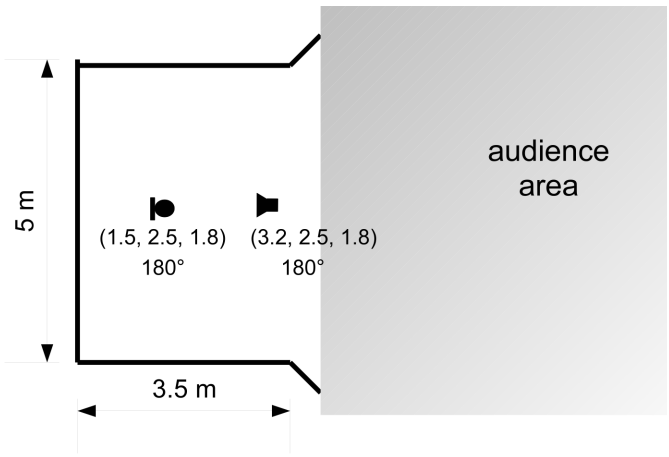

Fig. 3.30: Stage monitoring setup, example 1

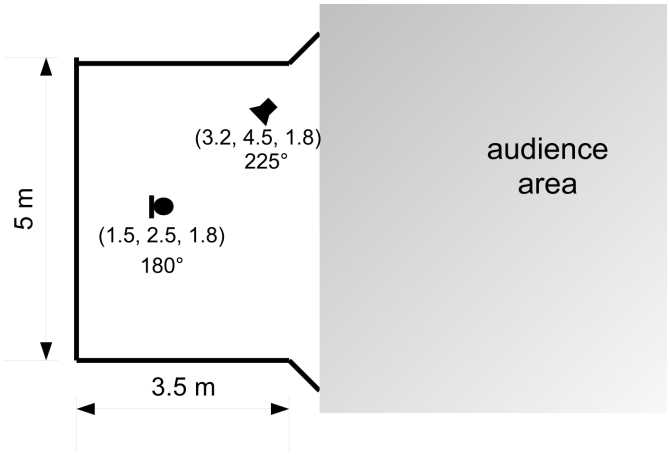

Fig. 3.31: Stage monitoring setup, example 2

Microphone	**MSG [dB]**	**F_{peak} [Hz]**
AKG D7	9.85	12712
AKG C480	9.70	8634
AKG CK98	9.46	125
Shure SM58	8.75	9268
AKG P5	7.87	3972
Neumann KMS105	7.30	9241
Shure KSM9	6.36	9684

Tab. 3.9: MSG and peak frequencies for Example 1

Judging simply from the setup of the first example, one could say, that for this array, a cardioid microphone is most suitable, since it has the best rejection of the direct sound entering at 180 degrees. Yet, the Shure KSM9, a cardioid microphone, has the lowest maximum stable gain. An explanation can be found, when analyzing the angle-dependent frequency responses. The KSM9 exhibits a strongly boosted sensitivity around 9.6 kHz at the 180° response [Fig. 3.32], which is the area where the peak of the loop transfer function was detected. In this range, the rejection is less than 5 dB compared to the on-axis.

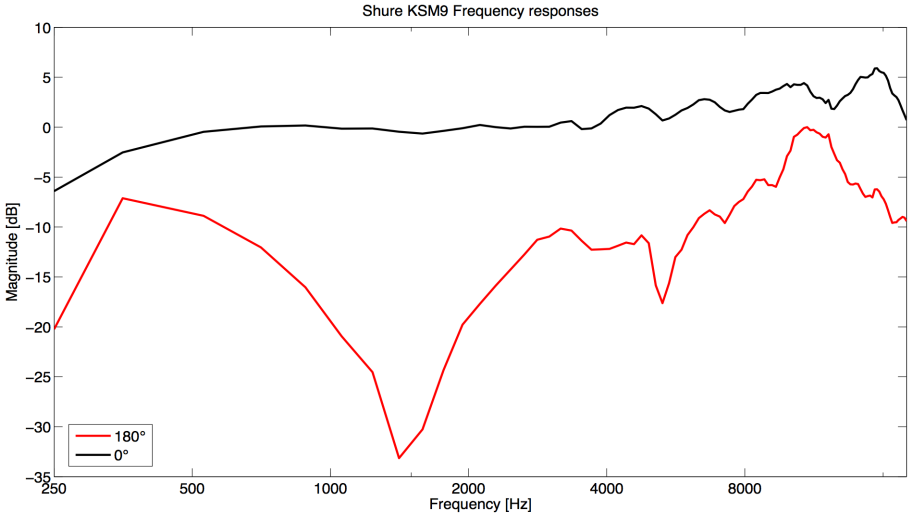

Fig. 3.32: Shure KSM9 - 0° and 180° frequency responses

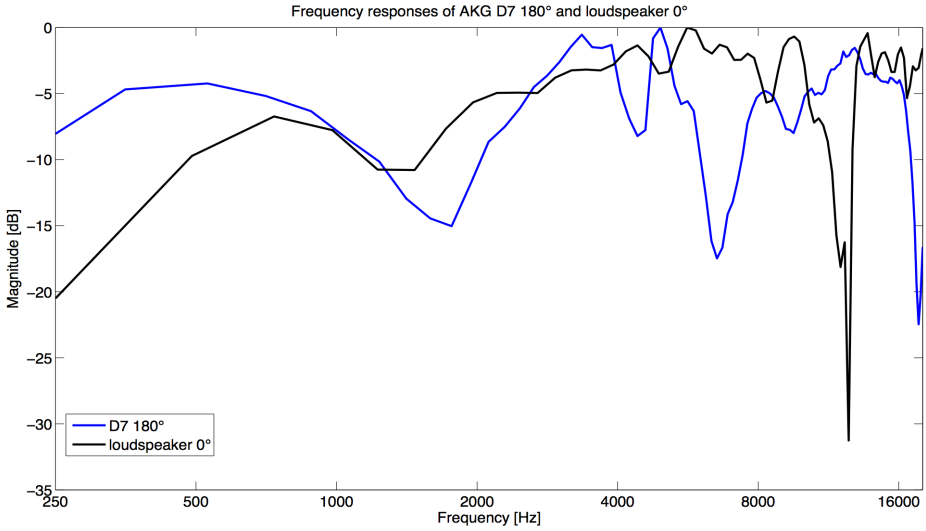

Fig. 3.33: AKG D7 and loudspeaker main path frequency responses

A similar explanation can be found for the good performance of the AKG D7. Looking at the frequency responses of the direct path, namely the loudspeaker at 0° and the microphone at 180°, it can be seen, that for this setup, microphone and loudspeaker have various complementary curves. Hence, a higher gain before instability can be applied than for a flat frequency response at 180°. For practical purposes, it is though difficult to anticipate such a behavior, which is in most cases purely coincidental.

Microphone	MSG [dB]	F_{peak} [Hz]
AKG CK98	7.49	3946
AKG C480	6.90	8568
Shure SM58	6.82	8133
Neumann KMS105	6.27	5243
AKG D7	5.89	5456
Shure KSM9	4.44	9509
AKG P5	4.12	4356

Tab. 3.10: MSG and peak frequencies for Example 2

The results of the second example show a very different ranking after the modification. The angle of the incoming direct sound is now at 130° at the microphone directivity pattern. Still, there is no clear tendency toward super-cardioid microphones showing better results. Due to the higher influence of the image sources and the diffuse field, more factors are involved and it becomes more complex to analyze the reasons for a good or poor performance of the various microphone types. Regarding the divergence of the results for both setups, it turns out there seem to be no hard and fast rules to classify a certain microphone as feedback prone or resistant.

Concluding, the feedback behavior of microphone types seems to be determined by several factors: The directivity and frequency characteristics as well as the locations and the resulting combination of angle-dependent microphone and loudspeaker and frequency responses. It is also interesting to point out that there was no tendency observable that condenser microphones are more feedback prone than dynamic

microphones.

3.11. Influence of the proximity effect

The low frequency enhancement due to the proximity effect is an interesting factor in the feedback network, since it only applies to the direct source placed close to the microphone. Reflections arriving at the microphone will not again experience the low frequency gain. This part of the transfer function is not part of the loop and does therefore not contribute to the limitations of the maximum gain before instability. [Fig. 3.34] shows the difference in the overall transfer function of the Shure SM 58 in the stage monitoring example 1 with a gain slightly below the feedback limit. This microphone was chosen since it has a relatively strong proximity effect, which can even be noticed slightly above 1kHz.

Even if the shape of the overall transfer function is not desirable and especially the frequency range below 500 Hz would have to be attenuated using a low shelving filter, the proximity effect causes a higher energy of the output signal, also in the useful range for speech between 500Hz and 2kHz. Consequently, a close spacing to the source does not directly yield a higher maximum stable amplifier gain, but the directional microphones deliver a higher output level at low frequencies. This useful acoustic gain does not affect the feedback path.

Going a step further, not only the bass enhancement has to be considered, but the entire on-axis frequency response both microphone $M_{close}(0)$ and loudspeaker S(0) for the direct electroacoustic path. For this extended signal path, the overall transfer function can be rewritten as:

$$H = \frac{S(\Phi = 0) \cdot M_{close}(\Phi = 0) \cdot g}{1 - L \cdot g} \quad . \tag{3.10}$$

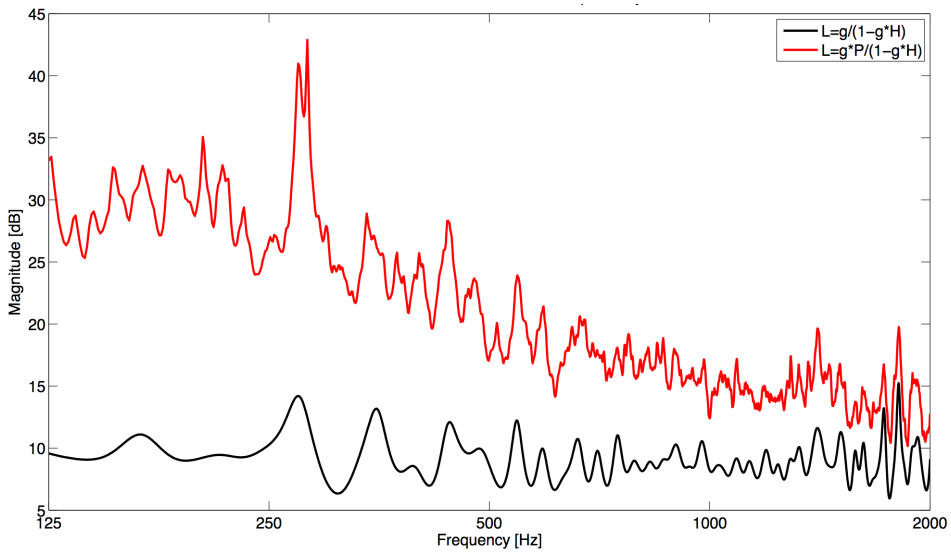

Fig. 3.34: Overall transfer function with and without proximity effect

[Fig. 3.35] shows the overall transfer function when the microphone and loudspeaker on-axis transfer functions are considered. The lower level results from the assumption, that the loudspeaker itself does not amplify and is therefore normalized to its maximum on-axis value.

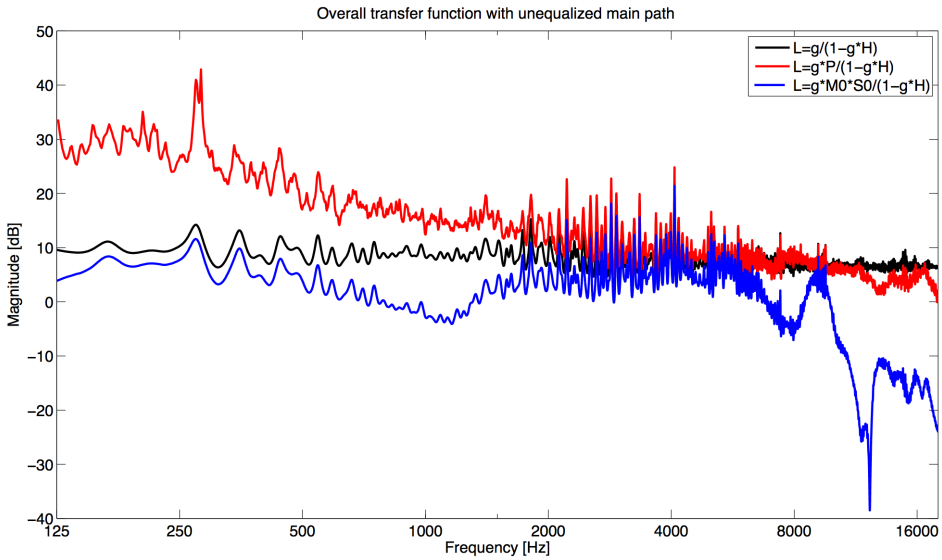

Fig.3.35: Overall transfer function with microphone and loudspeaker on-axis response

It can still be seen, that due to dips in the microphone and loudspeaker frequency

responses for certain frequency ranges a higher gain is necessary to obtain a flatter frequency response, as in this example around 1 kHz.

Chapter 4

CONCLUSION AND OUTLOOK

Summary

A simulation approach has been introduced, which made it possible to investigate the occurrence and properties of acoustic feedbacks in simple rooms, especially regarding various components of the feedback network.

Analyzing the phase of the loop transfer function confirmed, that the magnitude criterion gives a good estimation of the maximum stable gain and the feedback prone frequency range. Furthermore, the overall transfer function of the feedback network showed that gain values slightly below feedback, cause howling resonances in this frequency range, which become audible. The principle of equalization of the loop frequency response has been elucidated by showing the effects on the overall transfer function.

Varying the level of detail in the simulation gave some insight into relevant details for the calculation of MSG and feedback frequency. The resulting error is summarized in [Tab. 4.1] giving MSG values for a monitoring setup simulated at different levels of detail.

Simulation component	ΔMSG [dB]
Phase of microphone and loudspeaker frequency response	+ 0.01
Phase of microphone and loudspeaker frequency response and time delay of arrival	- 1.23
Second order image sources	+ 3.48
Diffuse field	+ 4.3

Tab. 4.1. Influence of simulation components on the calculated MSG

While the phase information of loudspeaker and microphone frequency responses turned out to be of minor importance, the consideration of the second order image sources as well as the time delay of arrival seems to be crucial for accurate simulation results. Especially for reverberant environments, modeling of the diffuse field has proven to be important.

In addition, several simulation parameters have been varied to investigate the determining factors of the feedback behavior. Because of the higher level of early reflections, small rooms are more feedback prone, although there is no perfectly linear relation between room volume and resulting gain before instability. The influence of a drastic change of the room shape was comparably small, although due to the omission of room modes, the modifications might be different in practice. It was furthermore shown that strong absorbing material can yield a useful improvement of the maximum stable gain.

Parameter	**Variation**	**ΔMSG [dB]**
Room volume	90 m³ to 400 m³	+ 5.03 dB
Room shape	6m x 5m to 10m x 3m	- 0.55 dB
Wall surface material	Wallpaper to acoustic panels	+ 3.02 dB

Tab 4.2.: Variation of simulation parameters

The loop transfer function emerged to be robust towards small positional and rotational changes. Only small variations in the peak frequency were being observed. Here again, greater variations could occur in practice due to the influence of the room modes. It furthermore turned out that, especially in reverberant environments, due to the strong influence of image sources, a greater microphone to loudspeaker spacing does not always yield higher maximum stable gains.

Finally, the influence of microphone and loudspeaker characteristics on the feedback behavior was examined. First, it was generally shown that the angle-dependent frequency responses of both microphone and loudspeaker strongly determine the shape

of the loop transfer functions. With directional microphones a MSG than can be 10 dB higher is achievable compared to omnidirectional microphones. A subsequent comparison of microphones showed that the particular combination of microphone and loudspeaker frequency responses largely determines the propensity to a low MSG. The fact that a modified setup caused a different ranking of the microphone types indicates that it is hard to say that a particular microphone is always mor feedback prone or resistant than competing products. A decisive factor can though be found in the proximity effect: Although it does not have a direct effect on the maximum stable gain setting of the amplified signal, it acoustically boosts low frequencies of the forward signal.

Outlook

To obtain an accurate prediction of the feedback behavior for specific environments, such as fixed sound reinforcement installations, several extensions of the developed simulation would be necessary. Especially the room simulation itself could become more precise by augmenting it to arbitrarily shaped rooms and to allow a more detailed description of the wall surfaces. By including a room mode estimation, further conclusions about the robustness of the loop transfer function could be drawn. Another interesting field of interest is the influence of obstacles in the room, especially the sound source in front of the microphone. Finally, the diffuse field is only roughly modeled, which could be redefined in future works.

To review and improve the simulation results, an adequate measurement method has to be found to compare simulated and measured data.

APPENDIX A

Absorption coefficients for several wall surface materials

	Absorption coefficient α for mid frequency							
Material	**63 Hz**	**125 Hz**	**250 Hz**	**500 Hz**	**1000 Hz**	**2000 Hz**	**4000 Hz**	**8000 Hz**
Smooth brickwork, 10 mm deep pointing	0.08	0.08	0.09	0.12	0.16	0.22	0.24	0.24
16-22 mm wood facing	0.25	0.25	0.15	0.1	0.09	0.08	0.08	0.07
Plaster with wallpaper on backing paper	0.02	0.02	0.03	0.04	0.05	0.07	0.08	0.08
Heavy carpet	0.08	0.08	0.24	0.57	0.69	0.71	0.73	0.73
Curtains (0.2 kg/m2) hung 90 mm from wall	0.05	0.05	0.06	0.29	0.63	0.70	0.73	0.73
Glass, large panes of heavy plate glass	0.18	0.18	0.06	0.04	0.03	0.02	0.02	0.02
Audience on wooden chairs, 1 per sq. m	0.16	0.16	0.24	0.56	0.69	0.81	0.78	0.78
Deweton acoustic panels Type A (Helmholtz resonators)	0.22	0.22	0.72	0.53	0.42	0.62	0.55	0.55
Lignoform Quadrillo-Ceiling panel	0.39	0.39	0.85	0.55	0.63	0.60	0.52	0.52

Fig. A.1.: absorption coefficients

APPENDIX B

Microphone frequency responses

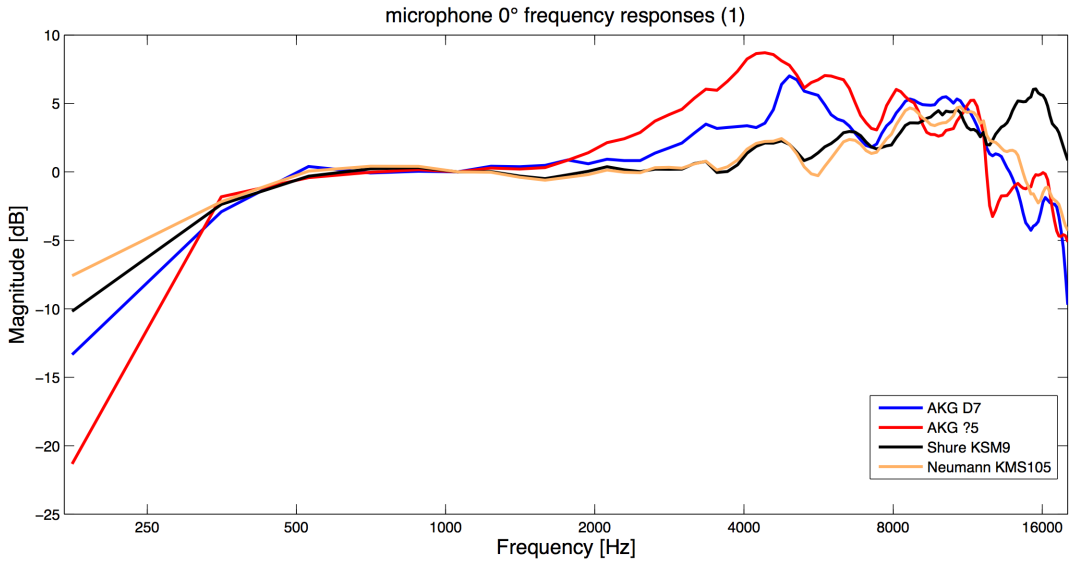

Fig. B.1.: on-axis responses for Shure KMS9, AKG D7, AKG P7 and Neumann KMS 105

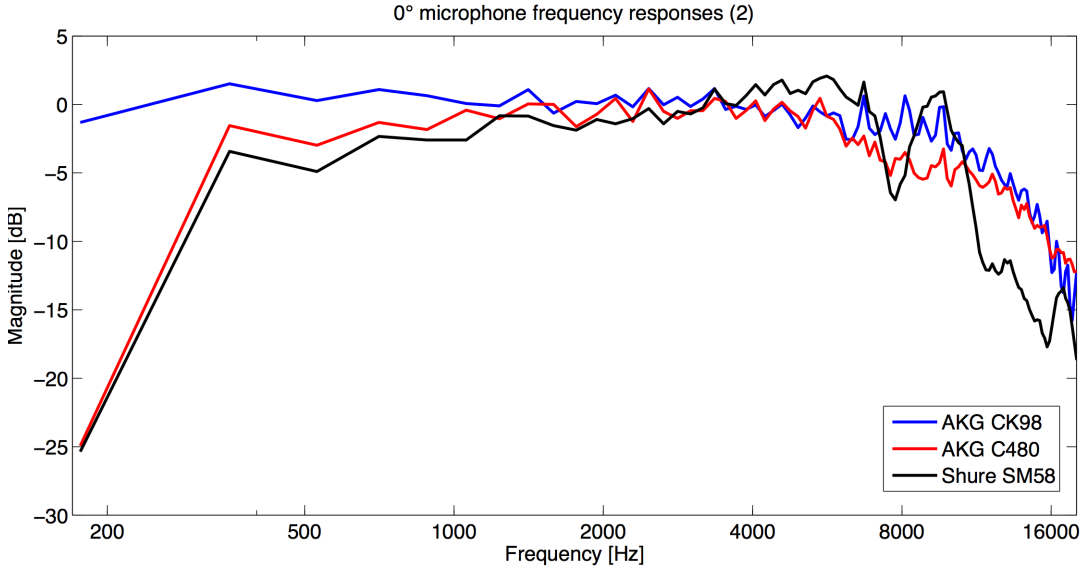

Fig. B.2.: on-axis responses for Shure SM58, AKG C480 and AKG SE 300 B

Microphone polar directivity patterns

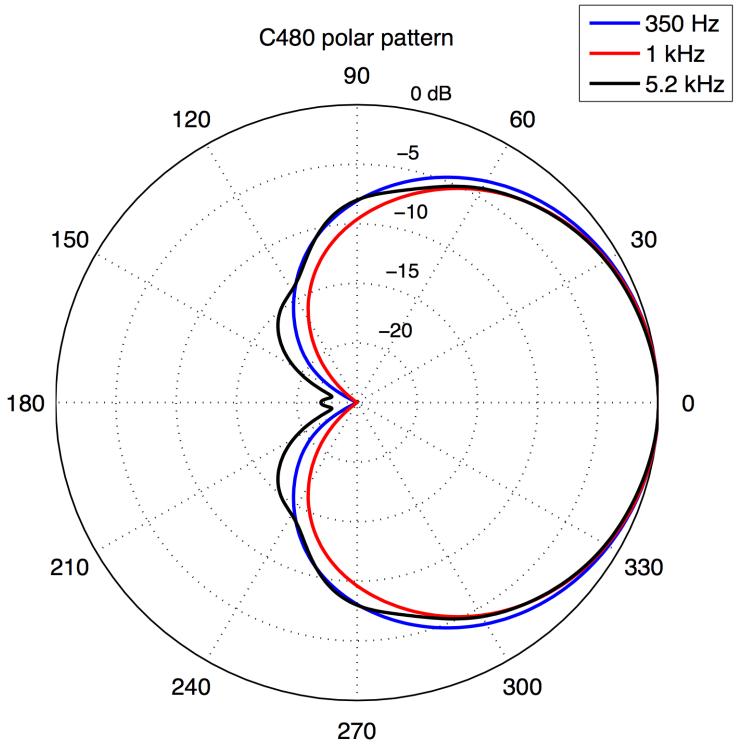

Fig. B.3.: directivity pattern AKG C480

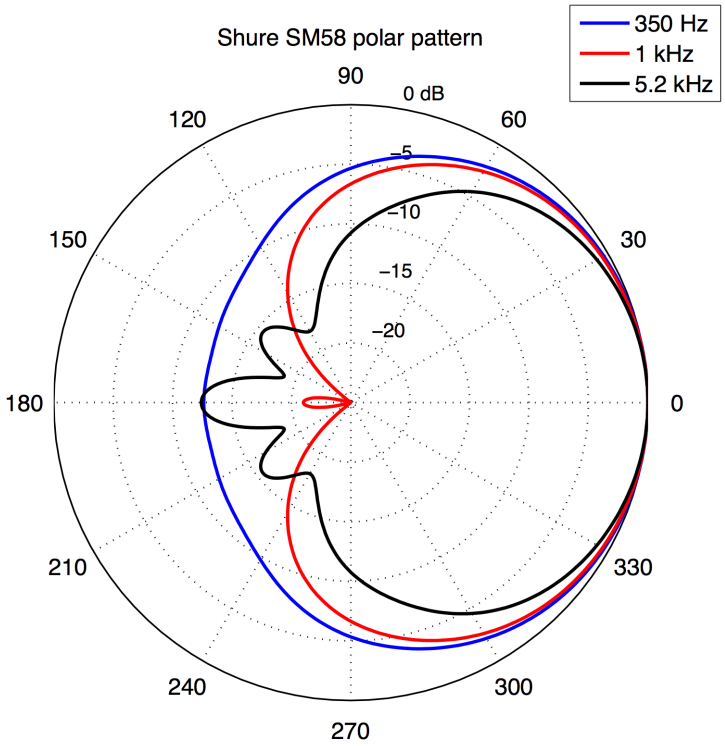

Fig. B.4.: directivity pattern Shure SM 58

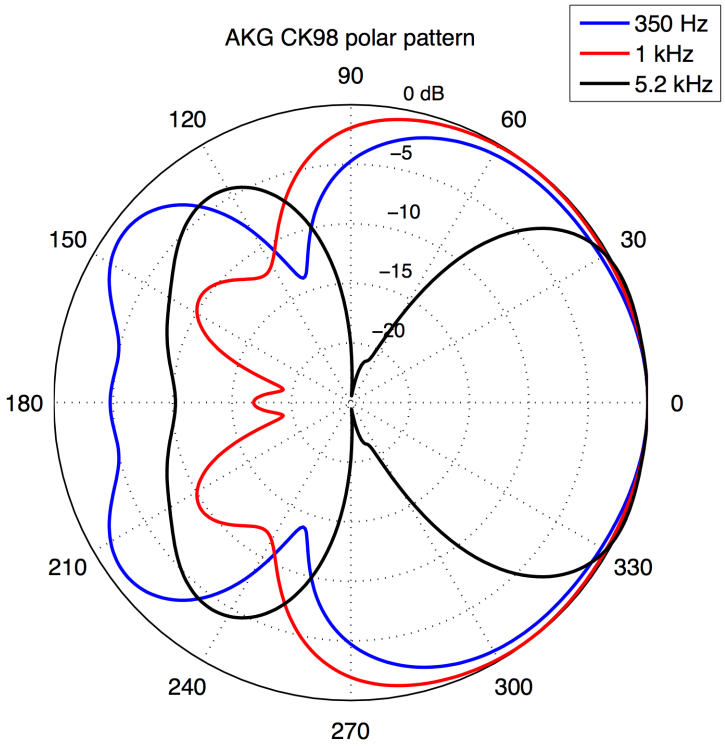

Fig. B.5.: directivity pattern AKG CK 98

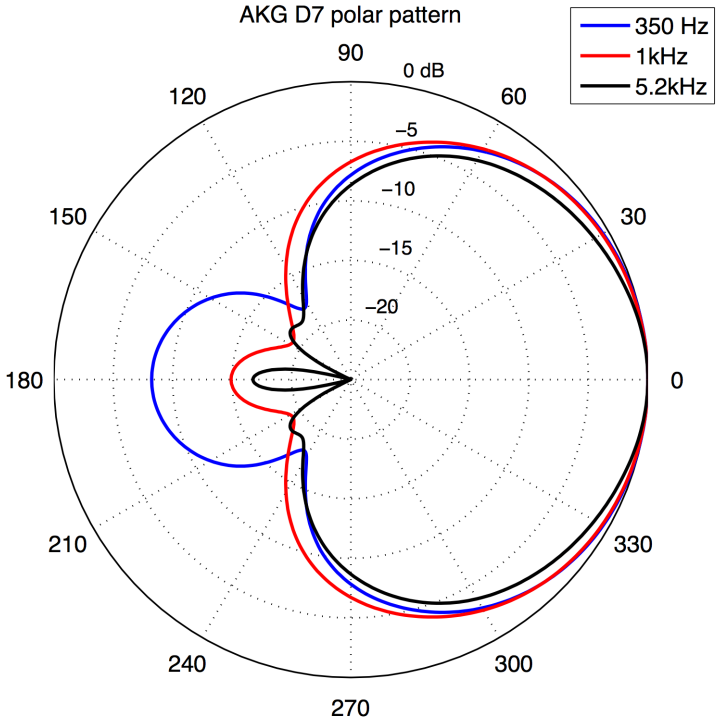

Fig. B.6: directivity pattern AKG D7

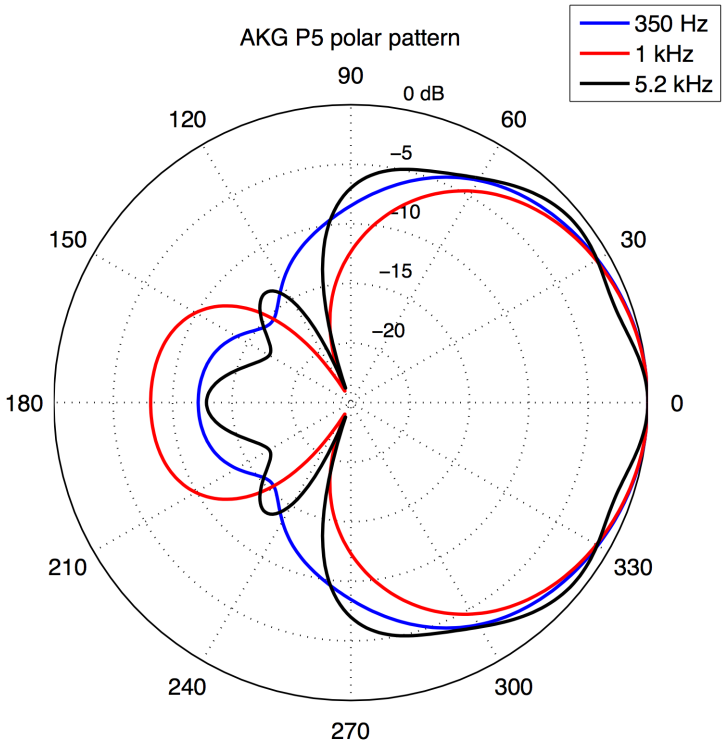

Fig. B.7: directivity pattern AKG P5

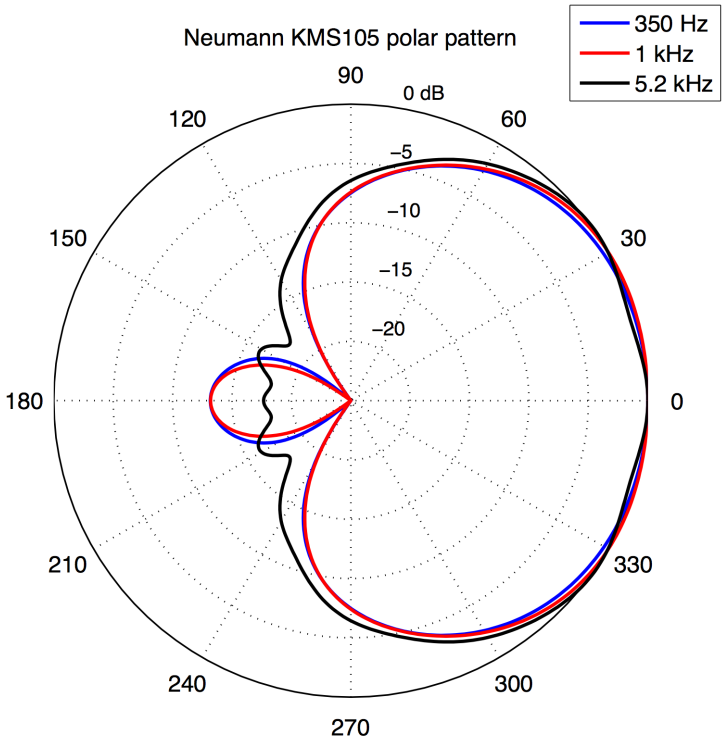

Fig. B.7: directivity pattern Neumann KMS 105

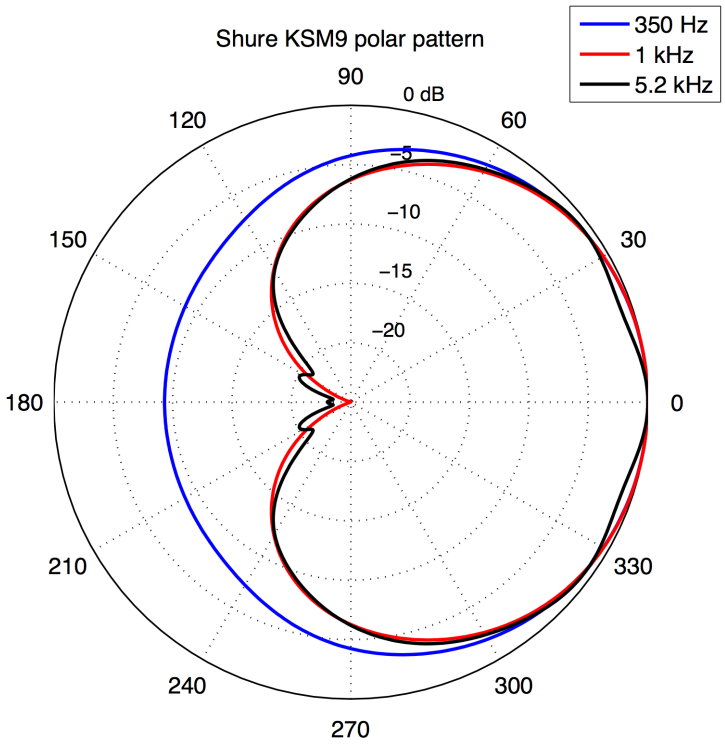

Fig. B.8: directivity pattern Shure KSM 9

Loudspeaker polar directivity pattern

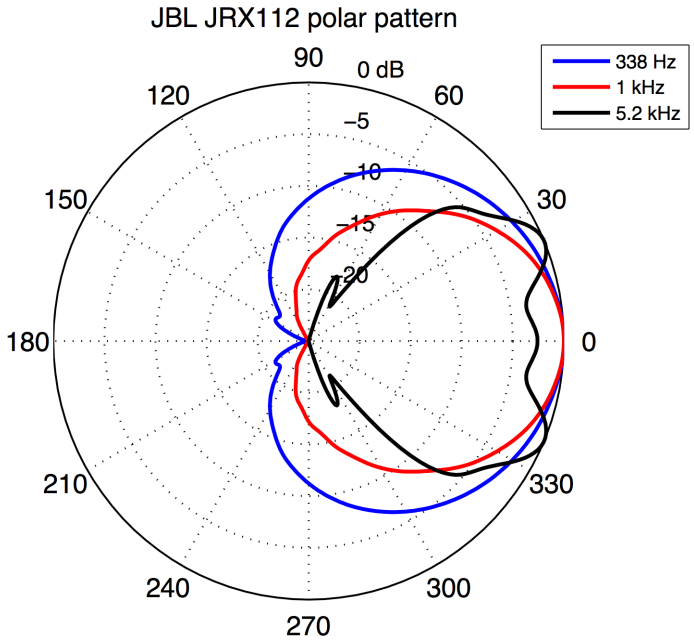

Fig. B.9: directivity pattern JBL JRX112

REFERENCES

[AB78] J. B. Allen and D. A. Berkley, „Image method for efficiently simulating small-room acoustics“, *Acoustics Research Department, Bell Laboratories, New Jersey,* June 1978

[BB66] C. P. Boner and C. R. Boner, „Behavior of Sound System Response Immediately Below Feedback“, *AES Journal, Vol.14, No.3, p. 200-203,* June 1966

[Cre78] L. Cremer, „Die wissenschaftlichen Grundlagen der Raumakustik, Band I“, *Hirzel*, Stuttgart, 1978

[Far07] A. Farina, „Advancements in impulse response measurements by sine sweeps“, *122nd AES Convention*, Vienna, May 2007

[FV03] W. Fasold and E. Veres, „Schallschutz und Raumakustik in der Praxis: Planungsbeispiele und konstruktive Lösungen“, *Beuth, Auflage 2.A.*, 2003

[Gol] Bob Golds, Collection of absorber parameters, available online: http://www.bobgolds.com/Sabin%20Data_sorted.htm

[HL03] D. Hayes and H. Luo, „Realtime Feedback Canceller“, *Unitron Hearing*, online brochure, www.unitron.com

[Kle73] D. Kleis, „Reduction of Acoustic Feed-Back in Sound System Applications“, *44th AES Convention, Rotterdam,* Feburary 1973

[Kre01] M. Krejci, „Entwicklung eines Mehrkanaligen Systems für eine virtuelle Raumakustik“, *Diploma Thesis, Institute of Electronic Music and Acoustics, University of Music and Performing Arts Graz*, October 2001

[Lit08] M. Litauer, „Der Nahbesprechungseffekt“, 2008, available online: *www.sengpielaudio.com/**NahbesprechungseffektLitauer**.pdf*

[LU10] R. Liepins and A. Ureta, „Messung von Abstrahlcharakteristika mittels Halbreis-Mikrofonarray“, *Laboratory report, Institute of Electronic Music and Acoustics, University of Music and Performing Arts Graz*, May 2010

[Mar06] D. Mariano, „Überblick über verschiedene Erklärungsansätze für das Zustandekommen des Nahbesprechungseffekts und Verifizierung derselben anhand der physikalischen Gegebenheiten im Schallfeld“, *University of Applied Science Mittweida*, 2006

[MM04] G. Müller and M. Möser, „Taschenbuch der theoretischen Akustik“, *Springer,* 2004

[ME98] P. Mapp and C. Ellis, „Improvements in Acoustic Feedback Margin in Sound Reinforcement Systems“, *105th AES Convention, San Francisco, California,* September 1998

[PL] S. C. Pei and H. S. Lin, „Minimum Phase Filter Design Using Real Cepstrum“, *Departement of Electrical Engineering, National Taiwan University*

[Sch71] R. B. Schulein, „Microphone Considerations in feedback-prone environments“, *41st AES Convention, New York,* October 1971

[TR09] M. Terrell and J. D. Reiss, „Optimising the re-enforcement effect of early reflections on aspects of live musical performance using the image source method“, *127th AES Convention New York,* October 2009

[WM09] T. van Waterschoot and M. Moonen, „50 Years of Acoustic Feedback Control: State of the Art and Future Challenges“, *Katholieke Universiteit Leuven, Departement Elektrotechniek*, ESAT-SISTA/TR 08-13, Feburary 2009

[Zot08] F. Zotter, „Uniform Sampling Strategies on the Sphere“, *Institute of Electronic Music and Acoustics, University of Music and Performing Arts Graz, Austria*, 2008